

1137  
113776

**NASA TECHNICAL MEMORANDUM 107619**

P. 42

**ENVIRONMENTAL FATIGUE OF AN Al-Li-Cu  
ALLOY: PART III - MODELING OF CRACK TIP  
HYDROGEN DAMAGE**

**Robert S. Piascik and Richard P. Gangloff**

**MAY 1992**



National Aeronautics and  
Space Administration

**Langley Research Center**  
Hampton, Virginia 23665

(NASA-TM-107619) ENVIRONMENTAL  
FATIGUE OF AN Al-Li-Cu ALLOY. PART  
3: MODELING OF CRACK TIP HYDROGEN  
DAMAGE (NASA) 42 p

N92-31215

Unclas

63/39 0113996



**ENVIRONMENTAL FATIGUE OF AN Al-Li-Cu ALLOY:  
PART III - MODELING OF CRACK TIP HYDROGEN DAMAGE**

**Robert S. Piascik and Richard P. Gangloff<sup>1</sup>**

**ABSTRACT**

*Environmental fatigue crack propagation rates and microscopic damage modes in Al-Li-Cu alloy 2090 (Parts I and II) are described by a crack tip process zone model based on hydrogen embrittlement.  $da/dN_{ENV}$  equates to discontinuous crack advance over a distance,  $\Delta a$ , determined by dislocation transport of dissolved hydrogen at plastic strains above a critical value; and to the number of load cycles,  $\Delta N$ , required to hydrogenate process zone trap sites that fracture according to a local hydrogen concentration-tensile stress criterion. Transgranular {100} cracking occurs for process zones smaller than the subgrain size, and due to lattice decohesion or hydride formation. Intersubgranular cracking dominates when the process zone encompasses one or more subgrains so that dislocation transport provides hydrogen to strong boundary trapping sites. Multi-sloped  $\log da/dN$ - $\log \Delta K$  behavior is produced by process zone plastic strain-hydrogen-microstructure interactions, and is determined by the  $\Delta K$  dependent rates and proportions of each parallel cracking mode ( $\Theta_i$ ) according to:*

$$da/dN_{ENV} \propto \Theta_{\{111\}} \Delta K^{2/\beta} + \Theta_{\{100\}} \Delta K^{(2 + 2\phi_{\{100\}})} + \Theta_{SGC} \Delta K^{(2 + 2\phi_{SGC})}$$

*Absolute values of the exponents and the preexponential coefficients are not predictable, however, fractographic measurements of  $\Theta_i$  coupled with fatigue crack propagation data for alloy 2090 establish that the process zone model correctly describes fatigue crack propagation kinetics. For example:*

$$da/dN_{Moist Air} = \Theta_{\{111\}} (3 \times 10^{-9}) \Delta K^{4.0} + \Theta_{\{100\}} (1 \times 10^{-8}) \Delta K^{5.1} + \Theta_{SGC} (2 \times 10^{-7}) \Delta K^{2.4}$$

*where each  $\Theta$  is known as a function of  $\Delta K$ . Crack surface films hinder hydrogen uptake to reduce  $da/dN$  and alter the proportions of each fatigue crack propagation mode.*

---

<sup>1</sup>Robert S. Piascik, formerly a graduate student in the Department of Materials Science at the University of Virginia, is a Scientist in the Mechanics of Materials Branch at the NASA-Langley Research Center, Hampton, VA, 23665. Richard P. Gangloff is Professor of Materials Science and Engineering at the University of Virginia, Charlottesville, VA, 22903.

## I. INTRODUCTION

A quantitative model for the kinetics of environmentally assisted fatigue crack propagation (FCP), based on mechanisms of crack tip damage, is central to alloy development and flaw tolerant life prediction<sup>(1,2)</sup>. Research reported in Part I characterized FCP in precipitation strengthened Al-Li-Cu alloy 2090 stressed in controlled inert (vacuum and helium), oxygen, and hydrogenous (pure water vapor, moist air and aqueous NaCl with varying polarization) environments<sup>(3)</sup>. These experiments produced intrinsic fatigue crack growth rate ( $da/dN$ ) versus stress intensity range ( $\Delta K = K_{max} - K_{min}$ ) data that are independent of crack closure and nonsteady-state chemical effects. A detailed fractographic analysis was presented in Part II; microscopic crack paths were defined and correlated with  $\Delta K$  and the underlying microstructure<sup>(4)</sup>. Those environments that are capable of producing atomic hydrogen on clean crack surfaces enhanced rates of FCP in 2090, and produced unique intersubgranular and transgranular  $\{100\}$  crystallographic fatigue cracking modes<sup>(3,4)</sup>. These observations were qualitatively explained based on hydrogen environment embrittlement.

The objective of the research in Part III is to understand and model the micromechanical and chemical bases for environmental FCP in Al-Li-Cu alloys. A framework is developed to model the relationship between  $da/dN$  and  $\Delta K$ , based on crack tip damage related to the interaction between dissolved hydrogen, plastic deformation and microstructure. The model is used to explain the effects of important variables including  $\Delta K$ , environment chemistry, microstructure and loading frequency.

### A. Background

The hydrogen embrittlement mechanism to enhance fatigue crack propagation in aluminum alloys exposed to moist air, water vapor and chloride electrolytes is based on broadly compelling, albeit circumstantial, evidence<sup>(2,5-32)</sup>. Atomic hydrogen is chemically adsorbed on clean crack surfaces as the straining aluminum alloy chemically reacts with gaseous  $H_2O$ , or after electrochemical cathodic reduction of hydrogen ions or water. Fatigue crack tip process zone damage is probably promoted by dissolved hydrogen through hydride formation, decohesion or localized plasticity based mechanisms<sup>(5,17,29,33,34)</sup>. Although evidence is lacking, environmental FCP mechanisms were proposed based on gaseous adsorption and crack surface film formation<sup>(12,35-37)</sup>. Adsorbed hydrogen or oxygen on the crack surface interact with strained atomic bonds to promote brittle fracture at lowered stress. Surface films may affect crack extension by inhibiting reversible slip, promoting slip homogenization, localizing the distribution and morphology of persistent slip

bands, or reducing crack tip welding. For alloys in aqueous electrolytes, a film formation/rupture/dissolution sequence was modeled to predict  $da/dN-\Delta K$ <sup>(12,38,39)</sup>, however, this approach has not been applied to aluminum alloys.

Quantitative models for hydrogen environment enhanced FCP kinetics must be based on one or more governing microscopic damage processes, and must integrate the mechanical and chemical components of crack tip damage. The mechanical contribution is described by relating the effective stress intensity to the continuum crack tip stress, plastic strain and strain rate fields<sup>(40-42)</sup>, and by determining the fracture process zone and damage sites. The chemical contribution requires modeling of occluded crack chemistry, crack surface reactions and hydrogen diffusion in the crack tip process zone<sup>(2)</sup>. Damage and  $da/dN$  depend on the amount of hydrogen delivered to the crack tip fracture process zone, and are described by a failure criterion between normal stress, strain and hydrogen concentration. Crack propagation occurs either per cycle or discontinuously after damage accumulation. To date, modeling has addressed either the crack chemistry of hydrogen production or crack tip plasticity damage without considering hydrogen; there is no integrated model for  $da/dN$  as a function of  $\Delta K$ , chemical and microstructural variables. Results in each regard provide the basis for the current modeling.

### **1. Mass Transport and Reaction Rate Limited FCP**

Hydrogen embrittlement models were developed to predict  $da/dN$ , as simply proportional to the amount of atomic hydrogen delivered to the crack tip fracture process site per single load cycle. These models hypothesize that  $da/dN$  is rate limited by one of the following: (a) environmental mass transport in the crack environment, (b) crack surface chemical or electrochemical reactions, or (c) hydrogen diffusion within the plastic zone. For the aluminum alloy-water vapor system, Wei and coworkers modeled  $da/dN$  based on slow mass transport within the occluded crack environment<sup>(2)</sup>. With limited exceptions, water vapor reactions on clean straining aluminum surfaces rapidly proceed to completion during a load cycle and are not rate limiting. Hydrogen production, and hence  $da/dN$ , are controlled by impeded molecular (Knudsen) flow within the crack, but only below a bulk environment "saturation pressure"<sup>(28,43,44)</sup>. Predictions of  $da/dN$  as a function of water vapor pressure, loading frequency and stress ratio (crack opening shape) are confirmed by experimental observations for several aluminum alloys, including 2090<sup>(3,28,43,45-48)</sup>.

The kinetics of hydrogen producing cathodic reactions on aluminum surfaces in aqueous electrolytes have not been characterized and related to environmental FCP<sup>(2,44)</sup>. For steels, Wei

and coworkers relate the corrosion fatigue component of  $da/dN$  to the amount of adsorbed atomic hydrogen produced per load cycle by cathodic  $H^+$  and  $H_2O$  reduction reactions, coupled with transient anodic dissolution<sup>(2,44)</sup>. Hydrogen production and  $da/dN$  are equated to the ratio of the anodic charge transferred per loading cycle and the amount associated with completed reaction of the clean surface. Charge transfer is measured in a fracturing electrode experiment<sup>(49)</sup>. This approach reasonably predicts the loading frequency dependence of corrosion fatigue crack growth for ferritic steels in electrolytes<sup>(2,44,49)</sup>. The model has not been applied to the aluminum alloy/aqueous chloride system where surface reaction rates are likely to be fast relative to typical loading frequencies<sup>(45)</sup>.

Contrary to the surface reaction model, environmental FCP rates may be controlled by atomic hydrogen diffusion within the cyclic plastic zone<sup>(6,50)</sup>.  $Da/dN$  is assumed to be proportional to the per cycle penetration distance of hydrogen ( $\Delta x$ ), and thus the square root of hydrogen diffusivity in aluminum and diffusion time (the reciprocal of the loading frequency). This relationship described the frequency dependence of the maximum crack growth rate where a hydrogen embrittlement induced intergranular to transgranular crack growth transition was observed<sup>(6,50)</sup>.

Chemically based crack growth rate models can predict the dependencies of  $da/dN$  on environmental activity (electrode potential, gas pressure and temperature) and time (loading frequency). The effects of  $\Delta K$ , mean stress and alloy microstructure are not described because  $da/dN$  is equated to hydrogen production, without considering process zone damage and the governing failure criterion. A critical assumption of the mass transport and reaction limited models is that the crack extends by a small increment per load cycle, however, there is no evidence to support continuous crack growth. Chemical models for hydrogen environment FCP do not address the uniquely damaging influence of cyclic deformation and the specific microscopic modes of process zone cracking.

## **2. Process Zone Plasticity Damage During FCP**

The interaction of cyclic plastic strain with microstructure and dissolved hydrogen near the crack tip must be understood to model environmental FCP behavior. Hydrogen volume diffusion in aluminum alloys is slow at room temperature, on the order of  $10^{-13}$  to  $10^{-15}$   $m^2/sec$ <sup>(19-21,51-55)</sup>, and may not support per cycle FCP over distances in excess of several  $\mu m$ . Arguments to the contrary were not proven<sup>(6,50)</sup>. Atomic hydrogen, residing in the cores of mobile dislocations, may sweep ahead of the straining crack tip up to  $10^4$  times faster than that enabled by

volume diffusion<sup>(17,26,27,54,56-58)</sup>. Enhanced grain boundary hydrogen diffusion was also proposed, although little evidence exists for this mechanism<sup>(51,56,59)</sup>. Boundary precipitates such as  $T_1$  are potential hydrogen traps that block a continuous diffusion path for hydrogen.

Process zone microstructure plays an important role in hydrogen embrittlement of aluminum alloys. During cyclic loading, dislocation cell structures and microvoids form as plastic strain accumulates and when microstructural barriers (grain and subgrain boundaries, precipitates, and dispersoids) interrupt the movement of dislocations<sup>(8,60-64)</sup>. Hydrogen atoms may segregate ("trap") at these fatigue induced sites<sup>(22-26,56-58,65,66)</sup>. Crack growth rate is enhanced when the crack path coincides with trap sites. Trap sites that shield the crack path from hydrogen segregation slow  $da/dN$ . Embrittlement of aluminum alloys is presumably enhanced by localized slip planarity that concentrates both hydrogen and stress<sup>(26,27,31,57,67)</sup>.

Considering mechanical fatigue damage based on plastic deformation at a crack tip, the unresolved issues are the precise nature of damage and the continuity of crack advance, be it per cycle or after accumulation over a number of load cycles<sup>(68,69)</sup>. For  $da/dN$  above  $10^{-4}$  mm/cycle, mechanical FCP is viewed to continuously occur during a load cycle and by a mechanical plastic blunting process that leads to microscopic striations. Laird proposed a crack blunting and buckling process for crack advance and resharpener<sup>(70)</sup>. Pelloux argues that continuous and striated fatigue crack growth in aluminum alloys is produced as alternating shear concentrates along  $\{111\}$  slip planes and symmetric about a resultant  $\{100\}$  crack plane<sup>(71)</sup>. Both ductile  $\{111\}$  and brittle  $\{100\}$  striations have been reported, however, the role of environment is unclear for each process<sup>(6,30,10,28,71-77)</sup>.

For  $da/dN$  below  $10^{-4}$  mm/cycle, Lankford and Davidson propose incremental crack extension by a two stage process involving crack tip strain accumulation, blunting and incremental crack extension over a number of loading cycles<sup>(8,68,78)</sup>. Incremental FCP was observed in 7075 and MA-87 aluminum alloys stressed at near threshold cyclic stress intensities ( $\Delta K_{th}$ ) in either moist air or nitrogen. The embrittling effect of moisture was ascribed to hydrogen which increased the increment of crack growth, and reduced the necessary failure strain and therefore the number of accumulated cycles for crack extension.

For discontinuous FCP, several models quantitatively predict  $da/dN$ - $\Delta K$  dependencies based on a microstructurally allowable length for slip<sup>(41,42,61,68,69,78)</sup>. The number of cycles for each increment of crack advance is given by a Coffin-Manson-type failure criterion based on crack tip plastic strain range. While consistent with  $da/dN$ - $\Delta K$  data for fatigue in embrittling

moist air, these models do not consider hydrogen effects and are not broadly tested with crack closure-free data for intrinsic FCP in an inert environment<sup>(68)</sup>. Growth rate models have not been developed based on damage by the interaction of hydrogen and cyclic plasticity.

### **3. Hydrogen Embrittlement and Cyclic Loading**

Time-cycle dependent environmental FCP occurs below the threshold stress intensity for monotonic load cracking in all aluminum alloy-water vapor and chloride systems including 2090<sup>(3,5,45)</sup>. Accordingly, cyclic loading and cyclic plastic deformation are uniquely damaging, as qualitatively explained by several hypotheses<sup>(5)</sup>:

1. Fatigue crack convective mixing enhances the transport of deleterious species from the bulk environment to the crack surface. Inhibiting species at the crack tip are similarly ejected.
2. Loading and unloading produce a sufficiently high crack tip strain rate to enhance film rupture, hydrogen production and hydrogen entry efficiency.
3. Cyclic plasticity continuously transports atomic hydrogen by the dislocation mechanism from the crack surface-environment interface to strong trapping sites within the embrittlement process zone.
4. Cyclic deformation produces crack tip dislocation cell or slip band structures that are strong trap sites and are embrittled by segregated hydrogen.
5. High normal stress is maintained throughout the crack tip field because of continued crack tip sharpening by cyclic unloading.

No model has been developed to quantify these explanations and to predict  $da/dN$  as a function of  $\Delta K$ , chemical and microstructural variables. The critical role of cyclic dislocation plasticity (items 3 and 4, above) is emphasized in the following model.

### **III. Process Zone Model For Hydrogen Environment Assisted FCP**

Since mass transport and reaction to produce hydrogen have been emphasized, it is important to consider the interaction of this hydrogen with the highly localized distributions of stress, strain, dislocation plasticity and microstructure in the crack tip process zone.

Presumably, hydrogen enhanced FCP discontinuously occurs over a distance ( $\Delta a$ ), defined as the embrittlement zone ( $d_{e,z}$ ), and after a number of elapsed load cycles ( $\Delta N$ ). The average crack growth rate is given by:

$$da/dN = (\Delta a/\Delta N) = d_{e,z}/\Delta N \quad (1)$$

where:

- $\Delta a$  = fatigue crack advance distance
- $\Delta N$  = load cycles required for crack advance; a function,  $g(\Delta\epsilon_p, \sigma_N, [H]_{pz})$ , of  $\Delta\epsilon_p$ ,  $\sigma_N$  and  $[H]_{pz}$
- $d_{ez}$  = embrittlement or damage zone length at the crack tip; a function,  $f(\Delta\epsilon_p, \sigma_N)$ , of  $\Delta\epsilon_p$  and  $\sigma_N$
- $\Delta\epsilon_p$  = crack tip plastic strain range; a function of  $r$ , the distance ahead of the crack tip
- $\sigma_N$  = crack tip stress normal to embrittled microstructure; a function of  $r$
- $[H]_{pz}$  = process zone atomic hydrogen concentration; a function of crack surface hydrogen concentration and crack solution electrochemistry.

This "damage accumulation" approach was employed to model mechanical FCP based on the coupling of the crack tip strain field (either continuum or experimentally defined) with a strain-based fatigue failure criterion such as the Coffin-Manson rule<sup>(8,41,42,78,79)</sup>. The physical bases and quantitative relationships for  $\Delta a$  and  $\Delta N$  are, however, likely to differ for FCP in hydrogen producing environments.

For FCP in Al-Li-Cu alloys, the role of crack tip cyclic plastic deformation is to enable dislocation transport of hydrogen to supply process zone embrittlement. For most growth rates, concentration gradient bulk diffusion is insufficient to sustain environmental FCP. For example, for a bulk hydrogen diffusivity ( $D_H$ ) of  $5 \times 10^{-15}$  m<sup>2</sup>/sec, diffusion throughout the cyclic plastic zone requires times equivalent to 60 load cycles for  $\Delta K = 2$  MPa $\sqrt{m}$ , 250 cycles for  $\Delta K = 3$  MPa $\sqrt{m}$  and 6,000 cycles for  $\Delta K = 7$  MPa $\sqrt{m}$ .<sup>2</sup> For all but the lowest  $\Delta K$  levels, these numbers of cycles exceed likely values of hydrogen reduced  $\Delta N$ . Since a diffusivity of  $10^{-10}$  to  $10^{-11}$  m<sup>2</sup>/sec is typical of dislocation transport of hydrogen in aluminum, particularly when slip is planar and localized, hydrogen rapidly penetrates the cyclic plastic zone; if mobile dislocation activity is sufficient<sup>(57)</sup>.

Atomic hydrogen is accumulated within the crack tip process zone by cyclic plastic strain, but brittle cracking is caused by the crack tip normal, or opening direction stress,  $\sigma_N$ . For fatigue crack advance,  $\sigma_N$  must be sufficiently high over the plasticity ( $\Delta\epsilon_p$ ) based distance where hydrogen has accumulated. This distance is defined as the embrittlement zone,  $d_{ez}$ . This view is assumed because normal stresses typically control interfacial (eg. SGC) and "cleavage" (eg. {100} crystallographic) cracking modes. Normal stress controlled FCP competes with cyclic

---

<sup>2</sup>The calculated cycles for hydrogen diffusion are based on elapsed time,  $t$ , at a loading frequency of 5 Hz and with the diffusion distance,  $2(D_H t)^{1/2}$ , equated to the cyclic plastic zone diameter,  $d_{cpz}$ . As discussed in Part II,  $d_{cpz}$  is reasonably approximated by the Rice-Irwin result:

$$d_{cpz} = (1/12\pi)(\Delta K/\sigma_{ysc})^2$$

with the monotonic yield strength,  $\sigma_{ys}$ , employed in place of the cyclic value<sup>(40)</sup>.

plastic strain-based damage, depending on the amount of process zone hydrogen and the level of  $\sigma_N$ .  $\Delta\epsilon_p$  depends on applied  $\Delta K$ , crack closure (if present), and material cyclic flow properties; while  $\sigma_N$  depends on  $K_{max}$  and material  $\sigma_{ys}$  and work hardening exponent,  $n$ . Analysis of Equation 1 to predict  $da/dN$ - $\Delta K$  is complicated because  $\Delta\epsilon_p$ ,  $\sigma_N$  and  $[H]_{pz}$  vary with distance ahead of the crack tip and with time during one or more load cycles, and the "f" and "g" functions are undefined. Material flow properties may depend on dissolved hydrogen. It is, none-the-less, informative to develop estimates for the crack advance distance and the number of cycles for discontinuous crack advance.

#### A. Determination of Crack Advance Distance - $\Delta a$

For hydrogen environment FCP, the crack advance increment ( $\Delta a = d_{cz}$ ) is determined by the distance ahead of the crack tip where cyclic plastic strain ( $\Delta\epsilon_p$ ) is sufficient to generate dislocation activity and enhanced hydrogen concentration. For heterogeneous planar slip materials such as aluminum alloy 2090, the nature of the dislocation cell structure is unclear<sup>(60,80)</sup>; the dominant process is assumed to be hydrogen transport by mobile dislocations to precipitate interface and subgrain boundary trapping sites.<sup>3</sup> The process zone model is simplified by the assumption that dislocation activity is defined by the peak plastic strain within the process zone. Differences in damage accumulation, that is dislocation activity and hydrogen concentration, associated with the crack tip strain gradient are not considered<sup>(41,79)</sup>.

Since significant plasticity is confined within a fraction of the crack tip cyclic plastic zone, it is reasonable to speculate that crack advance occurs over a fraction,  $\alpha$ , of  $d_{cpz}$ :

$$\Delta a = d_{cz} = \alpha d_{cpz} \quad (2)$$

Considering this plasticity condition for  $d_{cz}$ ,  $\alpha$  is defined by the critical plastic strain range ( $\Delta\epsilon_{p-crit}$ ) above which mobile dislocation activity is sufficient to transport H to trap sites. (Alternately, a critical strain may be required to produce a sufficient dislocation substructure for hydrogen trapping<sup>(81)</sup>.)  $\alpha$  is determined by equating  $\Delta\epsilon_{p-crit}$  to the continuum mechanics description of the (stationary, plane strain) crack tip plastic strain range,  $\Delta\epsilon_p$ , for the condition where  $r$  equals  $d_{cz}$  or equivalently,  $\alpha d_{cpz}$ . Since:

$$\Delta\epsilon_p = \omega(\sigma_{ysc}/E)[(d_{cpz}/r)^{1/(n+1)} - 1] \quad (3)^4$$

<sup>3</sup>For other alloys such as steels, a stable dislocation substructure is progressively formed by cyclic deformation. Hydrogen trapping at this substructure and associated microvoids may be dominant. Dislocation transport is not required for hydrogen in steels because of the relatively high hydrogen diffusivity of  $10^{-10}$  m<sup>2</sup>/sec<sup>(58,81)</sup>.

<sup>4</sup>Note that this continuum-based plastic strain distribution predicts a singularity at the crack tip where  $r$  equals 0.

where:  $\sigma_{ywc}$  = cyclic yield strength  
 $E$  = elastic modulus  
 $r$  = distance ahead of the crack tip  
 $n$  = work hardening exponent  
 $\omega$  = constant

solving for  $\alpha$  yields:

$$\alpha = [ \{ (\Delta\epsilon_{crit} E) / \sigma_{ywc} \} + 1 ]^{-1} \quad (4)$$

where:  $1/(n+1) = 1$  for peak aged aluminum alloys  
 $\omega = 1^{(40)}$

The continuum mechanics result in Equation 3 was experimentally demonstrated to describe the plastic strain distribution to within 1  $\mu\text{m}$  of the crack tip, at least for Fe-3%Si<sup>(40,82)</sup>. The result has not been verified for planar slip Al-Li alloys.

$\alpha$  depends on alloy microstructure, particularly if the cyclic deformation mode varies, and environment, if the brittle crack path changes. While this parameter cannot be unambiguously specified, various estimations discussed in Appendix A yield values of  $\alpha$  between 0.4 and 0.7.

Normal stresses are sufficiently high at all positions within the embrittlement zone and do not alter  $\Delta a$  determined by dislocation plasticity and  $\Delta\epsilon_{crit}$ . As shown in Appendix B, continuum analysis of the crack tip opening stress distribution within  $d_{cpz}$  indicates that  $\sigma_N$  at maximum load is constant and high (equaling 3 to 4 times  $\sigma_{ys}$ , depending on work hardening) over a distance of 3 to 250 times  $d_{ez}$ , for  $R$  values of 0.1 and 0.9, respectively. As applied  $K$  is cyclically varied from  $K_{min}$  to  $K_{max}$ , the maximum value of  $\sigma_N$  is unchanged, however, the extent of the stress field penetration within the process zone increases from a location very near to the crack tip (Equation B1 with  $K_{min}^2$ ) to the value given by Equations B1 and B2 in Appendix B. Unloading from  $K_{max}$  to  $K_{min}$  produces a compressive singularity, with near-crack tip compression depending on the extent of crack blunting and superimposed upon the tensile field. Dislocation motion may reverse in response to compressive yielding, however, this action does not alter the conclusion that tensile stresses within the plastic strain-based  $d_{ez}$  are sufficient to enable hydrogen cracking;  $\Delta a$  is defined by  $\epsilon_{p-crit}$  through  $\alpha$ .

### B. Determination of Failure Criterion - $\Delta N$

In the process zone framework,  $\Delta N$  is the number of load cycles required for dislocation transport to achieve a critical level of process zone hydrogen,  $[H]_{pz-crit}$ , for brittle crack advance over  $\Delta a$ . Here, failure occurs as a result of high  $\sigma_N$ . This view of  $\Delta N$  is stress-based and is fundamentally different from strain-based fatigue damage<sup>(8,41,42,78,83,84)</sup>. The challenge is to predict

$\Delta N$  as a function of  $\sigma_N$  and  $[H]_{pz}$ .  $[H]_{pz}$  depends on  $\Delta\epsilon_p$ , the absorbed crack surface hydrogen concentration ( $[H]_{ABS}$ ) in equilibrium with the occluded crack environment, alloy trap microstructure and fatigue dislocation trap structure. Hydrogen is delivered to process zone trap sites by dislocation motion during the loading portion of the fatigue cycle;  $[H]_{pz}$  increases with load reversals until the critical failure criterion between  $\sigma_N$  and  $[H]_{pz-crit}$  is achieved. Incremental crack growth occurs and the embrittlement process is repeated. The maximum value of  $\sigma_N$  is constant during load cycling. A finite number of load cycles is required to saturate relatively strong trap sites within the process zone because of limitations associated with "pickup" of atomic hydrogen at the crack tip surface-environment interface, with "deposition" of hydrogen as the mobile dislocation nears the trap, and because of the high hydrogen capacity of strong traps.

Qualitatively,  $\Delta N$  should decrease as the following factors increase:

1. Mobile dislocation density, which increases with increasing  $\Delta\epsilon_p$  and hence increasing  $\Delta K$ , and which depends on slip morphology;
2.  $\sigma_N$ , which is essentially constant with increasing  $\Delta K$ , but which increases with increasing  $\sigma_{ys}$  and  $n$ ;
3. Hydrogen environment activity and uptake efficiency which increase  $[H]_{ABS}$ ;
4. Damaging trap sites (e.g., subgrain boundary  $T_1$  precipitates, stable dislocation cells, localized slip bands and microvoids). An increased density of energetically beneficial traps increases  $\Delta N$ ;

It is not possible to present quantitative relationships that define  $\Delta N$  as a function of these factors. These relationships could be experimentally defined by low cycle fatigue-type experiments with notched and hydrogen precharged specimens. Such data have not been reported.

The load cycles for discontinuous crack extension can be estimated from measured crack growth rates for alloy 7075<sup>(3)</sup> and values of  $d_{cz}$  estimated through Equation 1. Figure 1 is a plot of this process zone model estimate of  $\Delta N$  compared with results calculated by a measurement and modeling approach applied to FCP in alloy 7075 in inert and hydrogen producing environments<sup>(8)</sup>. In this latter method,  $\Delta N$  is calculated from *in situ* SEM measurements of crack tip strain on the specimen free surface coupled with a Coffin-Manson criterion for the effect of plastic strain range on cycles to failure. The constants in the failure criterion were determined from  $da/dN$ - $\Delta K$  data.  $\Delta N$  was not directly measured by the SEM method. For the process zone estimates,  $\alpha$  values of 0.7 and 1 were used for moist air and vacuum, respectively.

The process zone model estimates for  $\Delta N$  shown in Figure 1 are in good agreement with

the SEM-based results<sup>(8,10)</sup>.  $\Delta N$  exceeds one, indicating discontinuous crack advance and  $\Delta N$  generally decreases with increasing  $\Delta K$ . The model and SEM results show fewer load cycles per crack advance event for moist air, an embrittling environment, compared to the inert environment. ( $da/dN$  for nitrogen containing 10 ppm  $H_2O$  are intermediate because low contaminant levels of  $H_2O$  are embrittling, as indicated by accelerated fatigue crack growth rates<sup>(3,9,45,85)</sup>.) Consistent with the previous discussion of slow hydrogen transport in aluminum, the small  $\Delta N$  values in Figure 1 suggest that bulk process zone hydrogen diffusion must be augmented by mobile dislocations to sustain rapid environmental FCP rates.

The specific  $\Delta N$  versus  $\Delta K$  relationship depends on the process zone failure criterion; for hydrogen producing moist air, damage is governed by  $[H]_{pz}$  accumulation and  $\sigma_N$ -based cracking, while FCP in vacuum progresses by a plastic strain-based damage process<sup>(42)</sup>. Specific functional relationships between  $\Delta N$  and  $\Delta \epsilon_{p-crit}$  are proposed in an ensuing section which discusses the relationship between  $da/dN$  and  $\Delta K$ .

## IV. Discussion

### A. Summary of Environmental FCP in Al-Li-Cu Alloy 2090

Table 1 summarizes the microscopic crack paths, and the associated  $da/dN$ - $\Delta K$  power law relationships for alloy 2090 in various environments, as reported in Parts I and II<sup>(3,4,45)</sup>. The {111}, subgrain boundary (SGC) and crystallographic {100} cracking modes are listed by increasing environmental susceptibility; vacuum, helium and oxygen, all produce equally slow  $da/dN$ ; followed by moist air, water vapor and anodic NaCl which promote the faster FCP rates. For nonhydrogenous vacuum, helium and oxygen, a single {111} cracking mechanism is observed and  $da/dN$  is characterized by a single  $\Delta K^{4.0}$  power law. For hydrogen producing moist air, water vapor and aqueous NaCl, changes in the  $da/dN$ - $\Delta K$  relationship are associated with different proportions of brittle SGC and {100} cracking. At low  $\Delta K$ , where a  $\Delta K^{5.1}$  power law is observed for both anodic NaCl and moist air, only transgranular {100} cracking is observed. SGC occurs at moderate to high  $\Delta K$ ; this fracture mode is described by a single slope power law of  $\Delta K^{2.7}$  for anodic NaCl and  $\Delta K^{2.4}$  for water vapor. Slip plane cracking is produced at high  $\Delta K$  for the aggressive environments. Complex changes in the  $da/dN$ - $\Delta K$  slope correlate with multiple fracture modes. For example, the  $da/dN$ - $\Delta K$  transitions and apparent "plateau" observed for 2090 in moist air at moderate to high  $\Delta K$  are associated with varying proportions of {100}, SGC and {111} slip plane cracking.

**Table 1: Environmental Fatigue Cracking in Alloy 2090<sup>3,4</sup>**

<u>Environment</u>	<u>Region A<sup>1</sup></u> <u>Low <math>\Delta K</math></u> <u>(<math>\leq 2</math> MPa<math>\sqrt{m}</math>)</u>	<u>Region B<sup>1</sup></u> <u>Moderate <math>\Delta K</math></u> <u>(3 to 7 MPa<math>\sqrt{m}</math>)</u>	<u>Region C<sup>1</sup></u> <u>High <math>\Delta K</math></u> <u>(<math>\geq 10</math> MPa<math>\sqrt{m}</math>)</u>	<u>Comments</u>
Vacuum .....	{111}	{111}	{111}	$\Delta K^{4.0}$
Helium .....	{111}	{111}	{111}	$\Delta K^{4.0}$
Oxygen .....	{111}	{111}	{111}	$\Delta K^{4.0}$
Moist Air .....	{100}	{100}/SGC/{111}	SGC/{111} <sup>2</sup>	$\Delta K^{5.1}$ (low $\Delta K$ ) $\Delta K^{1.5}$ (mod $\Delta K$ ) $\Delta K^{3.7}$ (high $\Delta K$ )
Water Vapor .....	{100}	SGC	SGC/{111} <sup>3</sup>	----- $\Delta K^{2.4}$ (mod $\Delta K$ ) <sup>4</sup> $\Delta K^{2.4}$ (high $\Delta K$ ) <sup>4</sup>
NaCl (anodic) .....	{100}	SGC	SGC/{111} <sup>3</sup>	$\Delta K^{5.1}$ (low $\Delta K$ ) $\Delta K^{2.7}$ (mod $\Delta K$ ) <sup>4</sup> $\Delta K^{2.7}$ (high $\Delta K$ ) <sup>4</sup>

<sup>1</sup> Defined in Figure 13, Part II<sup>(4)</sup>.

<sup>2</sup> Increasing proportions of mechanical {111} cracking are observed with increasing  $\Delta K$ .

<sup>3</sup> Primarily SGC with small proportions of {111} cracking at high  $\Delta K$ .

<sup>4</sup> Single slope behavior based on a single fracture mode.

***B. The Effects of Mechanical, Microstructural and Chemical Variables***

Considering the environmental FCP behavior of alloy 2090 described in Parts I and II and summarized in Table I<sup>(3,4,45)</sup>, the hydrogen embrittlement process zone framework explains the measured  $\Delta K$  and environment activity effects on the microscopic crack path, and the complex relationship between  $da/dN$  and  $\Delta K$ .

**1. Why Does the Intrinsic Fatigue Cracking Mode Depend on  $\Delta K$ ?**

A key aspect of environmental FCP in Al-Li-Cu and other 2000 series aluminum alloys is the complex dependence of crack growth rate on  $\Delta K$ , but only for aggressive environments<sup>(3,4,45)</sup>. Mechanical explanations for this behavior; including crack closure, static mode cracking above  $K_{ISCC}$ , stress state, and slip barriers; are not important<sup>(3)</sup>. Rather, the relationship between  $da/dN$  and  $\Delta K$  is governed by  $\Delta K$ -induced transitions in the microscopic modes of hydrogen enhanced FCP.

The results in Table 1 (and in Figures 12 and 13 of Part II) establish that the microscopic mode transitions between Regions A, B and C are controlled by the interaction between the

embrittlement zone volume and the included microstructure. Unlike previous arguments based on slip damage of unspecified form over a critical distance<sup>(38,62,63)</sup>, the process zone model suggests that microstructure controls hydrogen segregation by trapping and associated microcracking. Figure 2a is a scale drawing of the relationship between the L-T crack tip process zone ( $d_{cz} = \alpha d_{cpz}$ ) and the 2090 subgrain structure at high  $\Delta K$  (Region C). The average subgrain size of 5  $\mu\text{m}$  (transverse direction) is shown. At a  $\Delta K$  of 15  $\text{MPa}\sqrt{\text{m}}$  ( $K_{\text{max}} = 17 \text{MPa}\sqrt{\text{m}}$ ), the embrittlement zone volume ( $d_{cz} = 17 \mu\text{m}$ ) encompasses many subgrains in the crack growth direction and along the crack front. During cyclic loading, atomic hydrogen produced at the crack tip surface is transported by mobile dislocations to strong trap sites at subgrain boundaries within this large embrittlement zone. Bulk hydrogen diffusion is minimal at high  $\Delta K$  because few load cycles and a short time are required to hydrogenate the process zone by dislocation transport and to achieve the local failure criterion for discontinuous crack extension. In this regime mechanical slip band cracking competes with environmental SGC. Aggressive environments that produce high levels of crack surface hydrogen favor brittle intersubgranular cracking and little or no SBC. For less aggressive environments such as moist air, some SBC occurs, perhaps stimulated by hydrogen<sup>(31,57)</sup> and in parallel with SGC.

For near-threshold environmental FCP (Region A), embrittlement of subgrain boundaries is not possible because such boundaries are not hydrogenated by the localized dislocation activity associated with the small cyclic plastic strain-based process zone; Figure 2b. At these  $\Delta K$  levels,  $d_{cz}$  is not sufficiently large for dislocation transport of hydrogen to reach subgrain boundaries. In the absence of SGC, environmental FCP proceeds along  $\{100\}$  planes. As  $\Delta K$  increases, the embrittlement zone encompasses the smallest subgrains. The boundaries are enriched with hydrogen by trapping and the proportion of SGC increases while  $\{100\}$  cracking within subgrains decreases. The growth rate transition (A to B) and the beginning of SGC are expected at the  $\Delta K$  level where  $d_{cz}$  just equals the smallest subgrain size. Within Region B,  $\{100\}$  and SGC occur in parallel in proportions that are governed by the relationship between the distribution of subgrain sizes and the extent of dislocation transport within  $d_{cz}$ .

For Region A, a complication exists because both dislocation transport and bulk hydrogen diffusion may contribute to crack tip embrittlement due to the large number of load cycles, and the associated time, for each crack advance event. For example, the process zone model suggests that on the order of 200 load cycles are required to achieve the hydrogen-normal stress failure criterion and incremental crack growth over a relatively small advance distance (see Figure 1).

For a diffusivity of  $10^{-14}$  m<sup>2</sup>/sec, the diffusional penetration of hydrogen per increment of crack growth (e.g., 200 load cycles at a  $\Delta K$  of 2 MPa $\sqrt{m}$  and 5 Hz) is 1  $\mu\text{m}$ .  $D_H$  is uncertain and hydrogen diffusion may be slowed within  $d_{cz}$  by dislocation and microvoid traps in the highly strained plastic zone<sup>(58)</sup>. The {100} to SGC mode transition begins at that  $\Delta K$  level where dislocation transport occurs over a distance of the smallest subgrain diameter; but only for those cases where hydrogen supply by bulk diffusion is nil. This case is likely for high loading frequencies or fast crack growth rates (low elapsed time per crack advance event), and for low concentrations of crack surface hydrogen. When bulk diffusion of hydrogen is substantial within the process zone, intersubgranular cracking persists to  $\Delta K$  levels below the transition value from the plasticity consideration. The trends in Figure 13 (Part II) are consistent with these arguments. For a weak hydrogen environment such as moist air, SGC begins when  $d_{cz}$  equals the smallest subgrain size. SGC is observed for  $\Delta K$  and process zone size conditions that are smaller than the subgrain size for the aggressive NaCl environment. Above this transition, but for process zone sizes less than the subgrain size, dislocation transport augments bulk hydrogen diffusion, perhaps by translating the surface hydrogen source within the process zone and closer to, but not reaching, subgrain boundaries. The transition to {100} cracking and the Region A  $da/dN$ - $\Delta K$  dependence indicate that bulk diffusion is insufficient to supply subgrain boundaries below a transition  $\Delta K$  level and process zone size. Since monotonic load environmental cracking does not occur at the stress intensities where FCP is affected by the bulk hydrogen diffusion mechanism, cyclic loading is critical. In the absence of dislocation transport control, cyclic deformation may be required to destabilize crack surface protective films, thus promoting cathodic hydrogen production and entry efficiency.

## **2. Why Does Hydrogen Promote {100} and Intersubgranular Cracking?**

It is only possible to speculate on the origin of hydrogen enhanced {100} and intersubgranular cracking in alloy 2090; both microstructural features provide for local hydrogen trapping and therefore preferential fracture. Hydrogen trapping in complex aluminum alloys is poorly understood compared to steels<sup>(58,86-88)</sup>. High angle grain boundaries; dislocation structures and microvoids from fatigue damage; incoherent interfaces between the aluminum matrix and constituents, dispersoids or overaged precipitates; and somewhat more coherent interfaces associated with segments of strengthening and subgrain boundary precipitates are likely sites for irreversible hydrogen trapping in Al-Li-Cu-Zr alloys. Coherent interfaces, typical of unrecrystallized subgrains, under to peak aged intragranular precipitates, and isolated dislocation cores are

weaker reversible trap sites<sup>(58,86)</sup>. These later sites contain hydrogen in equilibrium with lattice dissolved solute and will yield hydrogen to stronger traps.

Considering the SGC mode, it is reasonable to speculate that low misorientation angle subgrain boundaries decorated with  $T_1$  precipitates<sup>(4)</sup> provide effective sites for hydrogen trapping. The strength of the subboundary- $T_1$  trap cannot be assessed, however, it is likely to be of moderate strength<sup>(32,87)</sup>. Hydrogen may be trapped at the incoherent ends of  $T_1$  plates along subboundaries. The subgrain boundary may trap hydrogen, without  $T_1$ , because of interfacial disorder or lithium solute segregation. As fatigue plasticity and damage accumulate at subgrain boundaries and  $T_1$ , including within the soft  $\delta'$  precipitate free zone, the strength of trap sites increases and perhaps approaches irreversibility. Subgrain boundary  $T_1$  is a stronger trap site than intragranular  $T_1$  and  $\delta'$ , because of the more disordered interface and localized fatigue damage, and is stronger than dislocation trap sites<sup>(86)</sup>. Mobile dislocations will therefore transport hydrogen from the crack-environment interface, through precipitation hardened aluminum grains, to subgrain boundaries where the solute is deposited at the stronger trap sites. FCP occurs along the subgrain boundary path because the localized failure criterion between hydrogen concentration and normal stress is achieved at such sites because of hydrogen segregation.

Subgrain boundary  $T_1$  is likely to anodically dissolve in an aluminum matrix, and to concomitantly stimulate local atomic hydrogen, entry when such boundaries intersect the crack surface and encounter electrolyte<sup>(32,89)</sup>. This behavior could promote hydrogen enhanced SGC, however, it is not the governing factor because similar intersubgranular cracking is observed for 2090 in aqueous NaCl, very low pressure water vapor and moist air<sup>(3,4)</sup>. The absence of an electrolyte for the gaseous environments precludes  $T_1$  dissolution, but not hydrogen trapping.

The reason for hydrogen enhanced cracking along  $\{100\}$  planes is more problematic. This crystallographic fracture mode has been reported for stress corrosion cracking and corrosion fatigue in a variety of 2000 and 7000 series aluminum alloys (Section I, Part II)<sup>(4)</sup> and for constant load liquid metal embrittlement of Al-Cu alloys<sup>(90)</sup>. Meletis recently reported transgranular "cleavage" cracking for hydrogen precharged Al-Li-Cu, without specifying the crystallographic crack plane<sup>(32)</sup>. Brittle cracking along  $\{100\}$  habit planes, typical of Guinier-Preston zones or  $\Theta'$  precipitates in Al-Cu alloys, does not explain  $\{100\}$  cracking in 2000 and 7000 series alloys that contain precipitates with either  $\{111\}$  habit planes (e.g.,  $T_1$  or  $\Omega$ ) or that are spherical without a well defined planar interface with the aluminum matrix (e.g.,  $\delta'$ )<sup>(90)</sup>. A lattice decohesion mechanism provides a rational, but speculative, basis for  $\{100\}$  cracking.

Hydrogen may accumulate in octahedral lattice sites that lie within {100} planes in the aluminum lattice. The source of this hydrogen is short range diffusion (or "leakage") from the trapped accumulation on {111} slip planes in planar slip alloys such as 2090. Crystallographic cracking results from crack tip normal stresses acting on disrupted lattice bonding about {100} planes. Atomic bonding energies in aluminum are reduced by solute hydrogen<sup>(17)</sup>. Both hydrogen accumulation and local tensile stresses could be enhanced by a dislocation mechanism based on interacting {111} glide planes to produce unresolvable microvoid damage nominally oriented along {100} planes<sup>(71,91-93)</sup>.

The recent report of the LiAlH<sub>4</sub> phase, formed in alloy 2090 during cathodic polarization (-1500 mV<sub>scc</sub> in 3% NaCl with a hydrogen recombination poison) and kinetically stable at 23°C, provides a speculative explanation for environmental FCP by the {100} and SGC modes<sup>(94,95)</sup>. Submicron sized hydride plates appear to preferentially nucleate at δ (AlLi) precipitates, and by inference at T<sub>1</sub> precipitates, both within subgrains and at subgrain boundaries. The hydride is thermodynamically stable compared to common lithium bearing precipitates in Al-Li-Cu alloys. Subgrain boundary hydride provides a logical reason for preferred hydrogen localization and SGC within the crack tip process zone. Intragranular LiAlH<sub>4</sub> forms as plates on {100} habit planes in the aluminum matrix. TEM observations reveal that hydrides crack along {120} planes in the hydride and nearly parallel to {100} planes in Al<sup>(94,95)</sup>. No fractographic evidence was obtained during the current study to support a hydride-based mechanism and the original study did not demonstrate hydrides on the intersubgranular or transgranular "cleavage" surfaces produced by stress corrosion cracking in the 2090/NaCl system. None-the-less, extensive evidence demonstrates that hydrides are likely to form in Al-Li-Cu alloys<sup>(94,95)</sup>. The role of this phase in environmental FCP must be further evaluated.

The transgranular {100} cracking mode transitions to intersubgranular cracking because of the strength of subboundary-T<sub>1</sub> hydrogen traps. As ΔK increases so that the process zone just encompasses a substantial number of subgrains, hydrogen associated with the {111} slip plane and {100} trap sites redistributes to the stronger sites at subboundaries. Without hydrogen accumulation, {100} (and {111}, if operative) cracking does not occur. Without hydrogen redistribution to strong subboundary traps, {100} cracking would persist to high ΔK levels, in spite of the fact that the process zone intersects subgrain and grain boundaries. The transition from crystallographic to interface hydrogen cracking in aluminum alloys depends on both ΔK (d<sub>cz</sub>) and hydrogen partitioning between trap sites. Temperature will affect hydrogen trapping and the

operative crack path.

### **3. Why Does the Hydrogen Environment Affect the Functional Relationship Between da/dN and ΔK?**

The relationship between da/dN and ΔK for a hydrogen-producing environment is determined by the ΔK dependencies of Δa, ΔN and the proportions of the {100}, intersubgranular and {111} cracking modes. For each environment, one or more power-law relationships superimpose to define the crack growth kinetics law.

Since Δa equals  $\alpha d_{cpz}$  based on dislocation activity control of crack advance (Equation 1), Δa should increase with  $\Delta K^2$ , independent of the microscopic mode of hydrogen cracking. Specifically, from Equations 2 and 4, and  $d_{cpz}$  in Footnote 2:

$$\Delta a = \Delta K^2 \left[ \{ \Delta \epsilon_{crit} E + \sigma_{ys} \}^{(n+1)} / 12 \pi \sigma_{ys}^{(n+3)} \right] \quad (5)$$

Δa is determined only by the extent of mechanical slip within the process zone and is independent of hydrogen concentration and tensile stress,  $\sigma_N$ .

ΔN decreases with increasing crack tip dislocation activity that provides increased hydrogen uptake to the embrittlement zone, per load cycle and for a constant crack surface environmental condition. That is, the number of load reversals required to achieve the critical trapped hydrogen concentration for crack advance decreases as the dislocation density within the embrittlement zone increases. Based on this argument, it is reasonable to assume that ΔN inversely depends on the total number of mobile dislocations within the crack tip embrittlement zone volume,  $N_m$ , raised to some power,  $-\phi$ . Assuming that mobile dislocation density is proportional to plastic strain<sup>(96)</sup>,  $N_m$  is described by the integral of the plastic strain range distribution from the crack tip to  $d_{cz}$ . This calculation, summarized in Appendix C, shows that:

$$\Delta N \propto \Delta K^{-2\phi} \quad (6)$$

This approach to estimating the ΔK dependence of ΔN is supported by the observation that intrinsic rates of environmental FCP generally depend on ΔK raised to a single power, at least for specific regimes of crack growth. The maximum crack opening tensile stress ( $\sigma_N$ ) in a load cycle depends on  $\sigma_{ys}$  and N, but not on ΔK; the stress aspect of the hydrogen failure criterion does not introduce an additional ΔK-dependent term. ΔN depends on the activity of the hydrogen environment. Combining the ΔK dependencies of Δa and ΔN yields:

$$\Delta a / \Delta N \propto \Delta K^2 / \Delta K^{-2\phi} \propto \Delta K^{(2+2\phi)} \quad (7)$$

Equation 6 describes the ΔK dependence of da/dN for a single microscopic damage process, however, macroscopic FCP rates can be determined by multiple concurrent damage

mechanisms. Wei and coworkers argue that the total environmental fatigue crack growth rate ( $da/dN_{ENV}$ ) equals the sum of the rates for individual mechanically and mechanical-chemically driven processes, that operate in parallel and each uniquely dependent on  $\Delta K$ , times the areal fractions ( $\Theta_i$ ) of each process<sup>(97)</sup>. For the case of alloy 2090 in the various environments:

$$da/dN_{ENV} \propto \Theta_{\{111\}}\Delta K^{2/\beta} + \Theta_{\{100\}}\Delta K^{(2 + 2\phi_{\{100\}})} + \Theta_{SGC}\Delta K^{(2 + 2\phi_{SGC})} \quad (8)$$

The first term describes mechanical FCP as typified by cyclic loading in vacuum. For this case, damage accumulation modeling predicts a power-law exponent of  $2/\beta$ , where 2 reflects the  $\Delta K$ -dependence of the crack tip plastic strain range (Equation 3) for a nonhardening alloy,  $\beta$  is the Coffin-Manson exponent employed as the failure criterion relating  $\Delta N$  to  $\Delta\epsilon_p$ , and crack advance occurs over a constant distance independent of  $\Delta K$ <sup>(41,83,84)</sup>. The  $\Delta K$ -dependent process zone perspective applied to purely mechanical fatigue predicts that  $\Delta K$  is raised to the power  $(2 + 2/\beta)$ .  $\beta$  has not been predicted from a damage model, but is measured to equal  $0.5 \pm 0.1$  for alloys. Accordingly, FCP in a truly inert environment should depend on  $\Delta K$  raised to between the fourth and sixth powers, depending on the  $\Delta K$ -dependence of the damage distance; an exponent of 4.0 is observed for alloy 2090 (Table 1)<sup>(3)</sup>. The second and third terms in Equation 8 describe  $\{100\}$  and intersubgranular cracking, respectively, with each uniquely depending on  $\Delta K$  through Equation 7.

When a single microscopic mode dominates FCP for a range of  $\Delta K$  values, as is the case for 2090 in NaCl with anodic polarization (Figures 12 and 13, Part II), the amounts ( $\Theta_i$ ) of the minority modes approach zero and  $da/dN$  depends on a simple power-law function of  $\Delta K$ . This case is idealized in Figures 3a and 3b for two constant levels of crack surface absorbed hydrogen concentration,  $[H]_{ABS1}$  and  $[H]_{ABS2}$ . Since Regions A and B/C correspond to predominantly  $\{100\}$  and SGC cracking, respectively, the  $\phi$  component of the power law exponent in Equations 7 and 8 must depend on the microscopic mode of cracking.  $\phi$ -values for  $\{100\}$  and SGC cracking (1.6 and 0.4, respectively) are calculated from the measured slopes of Region A and B/C (5.1 and 2.7, respectively, Table 1).

$\phi$  may depend on the microscopic cracking mode for two reasons. A constant amount of dislocation activity ( $N_m$ ) could differently supply hydrogen to the subgrain boundary and  $\{100\}$  fracture sites. That is, the efficiency of hydrogen transfer from dislocations to hydrogen traps at lattice and subboundary locations may vary. Hydrogen transfer between trap sites is likely to depend on the relative hydrogen binding energies for each site<sup>(58,87)</sup>, and on the dislocation structure on the active slip plane, which should vary with dislocation density and applied  $\Delta K$ .

Secondly, the critical concentration of hydrogen required for brittle crack advance, at a given  $\sigma_N$ , will vary for the two fracture mechanisms. The relationship between  $\Delta N$  and  $N_m$  will vary to reflect these physical processes.

#### **4. Why Does $[H]_{ABS}$ Affect the Magnitude and $\Delta K$ Dependence of $da/dN$ ?**

Comparison of FCP in NaCl (anodic polarization) to cracking in the moist gas and cathodic polarization chloride environments shows that decreasing environmental production of crack surface hydrogen results in reduced absolute crack growth rates, a more complex  $da/dN$ - $\Delta K$  dependence with "plateau" behavior, and increased transition  $\Delta K$  levels. This behavior is explained within the process zone framework and the assumption (Section B.6) that decreasing concentrations of absorbed atomic hydrogen are produced by Al surface reactions with NaCl (anodic polarization), water vapor, moist air and NaCl (cathodic polarization).

The number of load cycles required to achieve the critical level of process zone hydrogen, at a given  $\Delta K$  and hence mobile dislocation density, decreases with increasing crack surface absorbed hydrogen concentration in equilibrium with the local environment ( $[H]_{ABS}$ ). This hypothesis is based on the fact that the hydrogen capacity of strong traps within the process zone is independent of  $[H]_{ABS}$ ; with increasing  $[H]_{ABS}$ , decreased surface-to-trap site activity of dislocations ( $N_m$ ) is required to produce  $[H]_{crit}$ . Crudely, the product of  $[H]_{ABS}$  and  $N_m$  is constant. The increment of fatigue crack advance,  $\Delta a$ , is not affected by varying  $[H]_{ABS}$ . Figures 3a and 3b illustrate the simple effect of decreasing  $[H]_{ABS}$  on  $da/dN$ - $\Delta K$  when a single microscopic fracture mode operates. For FCP governed by dislocation transport of hydrogen (Figure 3a), decreasing  $[H]_{ABS}$  (from  $[H]_{ABS1}$  to  $[H]_{ABS2}$ ) depresses each power-law segment to lower  $da/dN$  at any  $\Delta K$  level; the transition  $\Delta K$  between  $\{100\}$  ( $\Theta_1 = \Theta_{\{100\}} = 1.0$ ) and SGC ( $\Theta_2 = \Theta_{SGC} = 1.0$ ) is not changed. Bulk diffusion may augment hydrogen transport during FCP at near threshold rates, as discussed in Section B.1. For the higher hydrogen activity environment, the dislocation and bulk hydrogen transport-based transition  $\Delta K$  shifts to lower values and the power-law segments increase at constant slope with increasing hydrogen uptake; Figure 3b.

#### **5. How Do Multiple Fracture Modes Affect The $da/dN$ - $\Delta K$ Relationship?**

For some hydrogen environments, two or more damage modes can operate in parallel over a range of  $\Delta K$ ; Equation 8 must be evaluated *in toto* and complex  $da/dN$ - $\Delta K$  relationships are likely. Fractographic results establish that multiple cracking modes occur when the hydrogen environment activity is reduced compared to anodic aqueous chloride. This result is reasonable because as  $\Delta N$  increases with decreasing  $[H]_{ABS}$  at any  $\Delta K$ , both SGC based on bulk hydrogen

diffusional supply and SBC based on mechanical damage accumulation assume increased importance. For multiple-mode FCP, the  $da/dN-\Delta K$  dependence suggested by Equation 8 is represented by the bold lines in Figure 3c. Each of the three possible microscopic cracking modes ( $\{100\}$ , SGC and  $\{111\}$ ) for alloy 2090 are associated with a single power-law  $da/dN-\Delta K$  relationship, as indicated by the dashed lines for unity values of  $\Theta_1$ ,  $\Theta_2$  and  $\Theta_3$ , respectively. As  $\Delta K$  increases,  $\{100\}$  cracking coexists with an increasing proportion of SGC; the two power-laws are added including increasing  $\Theta_2$  and decreasing  $\Theta_1$ . Since  $\{100\}$  cracking is characterized by a higher power-law exponent, the sum of the rates for the parallel processes may exhibit a maximum. When only SGC occurs ( $\Theta_2$ ),  $da/dN-\Delta K$  follows the single power law indicated by the short segment in Figure 3c. With further increases in  $\Delta K$ ,  $\{111\}$  SBC occurs and replaces SGC in increasing proportions. Since slip band cracking occurs at slower rates relative to intersubgranular FCP, Equation 8 indicates that  $da/dN_{ENV}$  follows one of the dashed bold lines, depending on the relative values of  $\Theta_2$  and  $\Theta_3$ . A single power-law  $da/dN-\Delta K$  relationship is produced when  $\Theta_3$  approaches unity, or when rates of SGC are inconsequential compared to slip band fatigue cracking. The concepts embodied in Equation 8 demonstrate the basis for complex  $da/dN-\Delta K$  relationships, including "plateau" behavior.

An example prediction of multiple fracture mode  $da/dN-\Delta K$  "plateau" behavior is demonstrated in Figure 4 for peak aged alloy 2090 in moist air. Here, measured<sup>(1)</sup> and predicted (Equation 8) intrinsic FCP rates are in excellent agreement. Predicted crack growth rate ( $da/dN_{ENV}$ ) is written in terms of the observed fatigue crack growth modes according to Equation 8:

$$da/dN_{Moist\ Air} \propto \Theta_{\{111\}}(da/dN_{Inert}) + \Theta_{\{100\}}(da/dN_{\{100\}NaCl}) + \Theta_{SGC}(da/dN_{Water\ Vapor}) \quad (9)$$

The second and third terms are empirically known because cracking in the 2090 was purely  $\{100\}$  for NaCl at low  $\Delta K$  and purely intersubgranular for water vapor at intermediate  $\Delta K$ .<sup>5</sup> Substituting the measured  $da/dN-\Delta K$  power-law exponent (Table 1) for each fatigue crack growth mode gives:

$$da/dN_{Moist\ Air} = \Theta_{\{111\}}(3 \times 10^{-9})\Delta K^{4.0} + \Theta_{\{100\}}(1 \times 10^{-8})\Delta K^{5.1} + \Theta_{SGC}(2 \times 10^{-7})\Delta K^{2.4} \quad (10)$$

with  $\Delta K$  in units of  $MPa\sqrt{m}$  and  $da/dN$  in mm/cycle. In contrast to the exponents, the power-law coefficients decrease with decreasing  $[H]_{ABS}$  (Figure 3a) and are not independently known. The values in Equation 10 were determined by fitting the portions of the moist air prediction to the

---

<sup>5</sup>It is equally valid to describe SGC by intermediate  $\Delta K$  FCP observed for NaCl, Table 1.

data in the  $\Delta K$  regimes where single cracking modes dominated.  $\Theta_i$  values were computed by a trial and error comparison of the data and model prediction in Figure 4. Figure 5 contains the distribution of  $\Theta$  values for {111}, {100} and SGC modes used to calculate  $da/dN_{\text{Moist Air}}$  in Figure 4. These distributions are reasonable based on fractographic estimates of  $\Theta$ 's for Regions A, B and C.

Quantitative fractography is required to verify the predicted fractions of each cracking mode shown in Figure 5, particularly in Region B where the proportions of each mode are complex and not easily discernable. The prediction in Figure 5 shows that complex  $da/dN$ - $\Delta K$  relationships are caused by varying proportions of microscopic cracking modes. While the power law exponent for each mode appears to be independent of hydrogen environment activity, the preexponential coefficients are not. Additional research is required to independently predict the effect of  $[H]_{\text{ABS}}$  on  $\Delta N$ , and hence the absolute values of  $da/dN$  at any  $\Delta K$ .

Multi-slope  $da/dN$ - $\Delta K$  and plateau crack growth rates are reported for environmental FCP in a variety of ferrous and 7000 series aluminum alloy-aqueous chloride systems<sup>(5)</sup>. Commonly, the transition  $\Delta K$  is associated with a change in the fracture mechanism, and the governing factor is argued to be mechanical (or stress intensity) rate limitation at low  $\Delta K$  and chemical (or hydrogen production and diffusion) limitation causing the plateau at higher  $\Delta K$ <sup>(6,50,81,98)</sup>. This notion is supported by the frequency independence of low  $\Delta K$  growth rates and by the strong frequency dependence of  $da/dN$  within the plateau for 7000 series aluminum alloys and steels<sup>(5)</sup>. For 2000-series alloys<sup>(5)</sup>, including alloy 2090<sup>(3)</sup>, in aqueous chloride and saturation pressure water vapor,  $da/dN$  does not increase with decreasing loading frequency (see Section IV.B.6.b). Accordingly, the complex  $da/dN$ - $\Delta K$  relationships depicted in here are not explained by chemical rate limitations. While the shape of the  $da/dN$ - $\Delta K$  law was ascribed to transitions in fracture mode, detailed measurements and models were not proposed<sup>(28,31)</sup>. The process zone framework, Equation 8, provides a rational explanation. When operative, rate limited environmental FCP further complicates the intrinsic  $da/dN$ - $\Delta K$  relationships predicted by the process zone model for multiple parallel cracking modes<sup>(2)</sup>. Additionally, extrinsic crack closure will complicate  $da/dN$ - $\Delta K$  laws for both inert and embrittling environments<sup>(99)</sup>.

## **6. Does the Process Zone Framework Explain the Effects of Hydrogen Environment Activity and Loading Frequency?**

Data in Parts I and II and the process zone damage framework suggest that decreasing concentrations of absorbed hydrogen on alloy 2090 crack surfaces are produced in order by NaCl

(anodic polarization), pure water vapor, moist air and NaCl (cathodic polarization).  $da/dN$ , the proportions of each microscopic cracking mode, and the  $da/dN-\Delta K$  dependence depend on  $[H]_{ABS}$ . For the moist gaseous environments, molecular transport modeling and experimentation establish that  $[H]_{ABS}$  and hence  $da/dN$  increase with: a) increasing exposure (water vapor pressure/loading frequency), but only up to a saturation level, b) increasing  $R$ , and c) decreasing oxygen partial pressure and blocking surface oxide<sup>(2,43,46-48)</sup>. These expectations are supported by FCP data for alloy 2090<sup>(3,45)</sup> and are consistent with the process zone concepts of dislocation transport and microstructural trapping of hydrogen. Process zone hydrogen diffusion does not limit FCP because of dislocation enhanced mass transport and the short diffusion distance over  $d_{ez}$ <sup>(6,50)</sup>.

Crack growth in aqueous chloride is qualitatively understood based on occluded crack electrochemistry and crack surface passive films that reduce hydrogen entry to the process zone.

**a. Electrode Potential:** For alloy 2090 in aqueous NaCl, the important result to explain is the substantial rates of FCP under anodic polarization compared to the inhibiting and crack arresting effects of cathodic electrode potentials<sup>(3)</sup>.

A schematic of crack tip electrochemical reactions is shown in Figure 6a. For anodic potentials near the free corrosion value, dissolution occurs under relatively surface film-free conditions and the resulting cations (predominantly aluminum) are hydrolyzed to decrease crack tip pH and increase hydrogen production by proton reduction<sup>(100-102)</sup>. As potential decreases, dissolution rates decrease,  $Al^{+3}$  hydrolysis is reduced, pH increases and  $[H]_{ABS}$  decreases, as indicated in Figure 6b. With decreasing potential, water reduction becomes the dominant source of hydrogen. The minimum in  $[H]_{ABS}$  correlates with monotonic load hydrogen cracking in aluminum alloys at both anodic and cathodic potentials<sup>(51,95)</sup>.

The complicating effect of a crack surface film must be considered for Al-Li alloys. At cathodic potentials, the increasingly alkaline crack solution produces a black surface film, possibly  $Al(OH)_3$  and  $LiOH$ <sup>(3)</sup>. Speculatively,  $LiOH$  hinders atomic hydrogen permeation into the process zone;  $[H]_{ABS}$  is lowered, thus explaining the beneficial effect of cathodic polarization. While reduced  $da/dN$  is explained based on either the chemistry argument represented in Figure 6, or by the film effect, the prolonged times for fatigue crack growth reinitiation when changing from cathodic to anodic potential<sup>(3)</sup> are evidence for the dominant effect of a protective crack tip surface film.

Within the context of the process zone model, the important conclusion is that cathodic

polarization reduces  $[H]_{ABS}$  for alloy 2090 in NaCl. Decreasing crack surface hydrogen concentration results in "plateau" behavior because: a) the magnitude of  $da/dN$  is reduced for both pure {100} and intersubgranular cracking, b) the {100} to SBC transition  $\Delta K$  increases because of decreasing bulk diffusion of hydrogen, and c) SBC is increasingly important at higher  $\Delta K$  when rates of SGC are reduced. This behavior is illustrated by the bold curve in Figure 3c.

**b. Loading Frequency:** Considering alloy 2090 in NaCl (anodic polarization), the important result to explain is that loading frequency ( $f$ ) has no effect on  $da/dN$  for near threshold  $\Delta K$  levels and that  $da/dN$  moderately increases with increasing frequency for higher  $\Delta K$ <sup>(3)</sup>.

The frequency dependence of  $da/dN$  for environmental FCP in aluminum alloys is determined by the kinetics of crack environment mass transport, chemical or electrochemical surface reactions and process zone hydrogen diffusion, and by crack tip strain rate effects on surface reactions, film stability and  $[H]_{ABS}$ <sup>(2,5)</sup>. The measured frequency dependencies of  $da/dN$  for alloy 2090 in aqueous chloride suggest that: (a) surface anodic dissolution and cathodic H production reactions progress to completion for the frequencies considered (0.07 Hz to 20 Hz) and (b) process zone hydrogen diffusion is fast during the multiple load cycles necessary for crack advance. Accordingly, environmental FCP in the 2090/NaCl system is not transport or surface reaction rate limited. Rather, we speculate that increased crack tip strain rate causes increased hydrogen production and/or uptake to reduce  $\Delta N$  and increase  $da/dN$ .

Fast surface reaction kinetics are consistent with results reported by Wei and coworkers for 7000 series aluminum alloys<sup>(2,28,44)</sup>. The process zone model suggests that hydrogen transport ahead of the crack tip is not rate limiting because of rapid dislocation transport and short diffusion distances,  $d_{ez}$ . For hydrogen transport in the process zone to be growth rate limiting, a loading frequency of 150 Hz or higher is required; based on a hydrogen diffusivity of  $10^{-10}$  m<sup>2</sup>/sec for dislocation transport, a process zone size of 7  $\mu\text{m}$  ( $\Delta K = 10$  MPa $\sqrt{\text{m}}$ ) and a  $\Delta N$  of 20 cycles. At low  $\Delta K$ , diffusion distances are smaller,  $\Delta N$  is larger, and extremely high loading frequencies (> 150 Hz) are required to limit process zone hydrogen diffusion. Stanzl et al. demonstrated that relatively high pressure pure water vapor accelerates low  $\Delta K$  FCP rates in 2024-T3, compared to vacuum, and at an ultrasonic loading frequency of 20,000 Hz<sup>(103)</sup>. A complex  $da/dN$ - $\Delta K$  relationship, including "plateau" behavior was reported.

At high  $\Delta K$ , a mild increase in fatigue crack growth rate with increasing loading frequency suggests that surface film destabilization promotes  $[H]_{ABS}$  and subsequent hydrogen ingress over  $d_{ez}$ . Average crack tip strain rate per loading cycle ( $\dot{\epsilon}_{CT}$ ) is proportional to  $\Delta K^\gamma f$ , where  $\gamma$  is

between 2.5 and 3.5 for 7075 fatigued in moist air<sup>(104)</sup>. As  $f$  increases at constant  $\Delta K$ ,  $\dot{\epsilon}_{CT}$  linearly increases and a film on the crack surface is disrupted more frequently per unit time, perhaps as a critical film rupture strain is exceeded<sup>(39)</sup>. If the in-tact film blocks cathodic hydrogen production or hydrogen atom entry to the process zone, then increased film disruption promotes increased hydrogen entry per unit time. That is,  $[H]_{ABS}$  increases with increasing loading frequency;  $da/dN$  accordingly increases as illustrated in Figure 3a or 3b.

The lack of a frequency effect at low  $\Delta K$  is reasonable because  $\dot{\epsilon}_{CT}$  values are substantially less than those of the high  $\Delta K$  case for the frequency range examined, and may not be sufficient for repeated film rupture. Surface repassivation would rapidly occur relative to the time interval between rupture events at the slow  $\dot{\epsilon}_{CT}$ . Hydrogen production and entry are not enhanced by increasing  $f$ . For  $\gamma$  equal to 3.0,  $f$  levels between 10 and 200 Hz are required to develop near- $\Delta K_{th}$  (2 MPa $\sqrt{m}$ ) crack tip strain rates equivalent to those produced at higher  $\Delta K$  (10 MPa $\sqrt{m}$ ) and  $0.1 < f < 5$  Hz. High frequency FCP was not examined for 2090 in aqueous chloride. At such high frequencies, dislocation transport will not limit  $da/dN$ , however, surface electrochemical reactions may become important and further complicate the effect of loading frequency. A corollary to this argument is that increasing  $\Delta K$  at constant frequency will strongly increase  $\dot{\epsilon}_{CT}$ , promote film instability, increase  $[H]_{ABS}$  and thus increase  $da/dN$ . The effect of stress intensity on crack surface hydrogen concentration was not considered in the development of the process zone model prediction of  $da/dN$ - $\Delta K$ ; Equation 8.

The scenario proposed for alloy 2090 is relevant to hydrogen environmental FCP in other 2000 series alloys that exhibit a similar frequency dependence<sup>(5)</sup>. The situation is more complex for 7000 series alloys where  $da/dN$  substantially decreases with increasing frequency. In this case surface reaction rate and surface film stability may both govern the frequency response, with the former dominating surface hydrogen production. There is no evidence to suggest that hydrogen diffusion is growth rate limiting for 7000 or 2000 series aluminum alloys, consistent with the process zone model.

## V. CONCLUSIONS

1. Environmental fatigue crack propagation rates and microscopic cracking modes, established in Parts I and II for Al-Li-Cu alloy 2090 in moist gases and aqueous chloride<sup>(3,4)</sup>, are explained by a crack tip process zone model based on hydrogen embrittlement. The macroscopic growth rate ( $da/dN_{ENV}$ ) is equated to *discontinuous* crack

advance over a distance ( $\Delta a$ ) determined by mobile dislocation transport of hydrogen at plastic strains above a critical value; and to the number of load cycles ( $\Delta N$ ) required to sufficiently hydrogenate process zone trap sites that fracture due to a local hydrogen concentration-tensile stress criterion.

2. The process zone model explains  $\Delta K$  and dissolved hydrogen-dependent fatigue crack path transitions. For Al-Li-Cu exposed to NaCl or moist gases at low  $\Delta K$ , FCP is along  $\{100\}$  planes due to H-induced lattice decohesion or hydride formation, and because the embrittlement process zone is smaller than the subgrain size; a single power-law  $da/dN$  versus  $\Delta K$  relationship results. When  $\Delta K$  increases to the level where the process zone just includes subgrains and dislocations reach such boundaries, environmental FCP transitions to the intersubgranular mode because of strong hydrogen trapping at subgrain boundary sites including  $T_1$  precipitates; a transition occurs in the slope of  $da/dN$ - $\Delta K$ . A second transition occurs at higher  $\Delta K$  when substantial slip plane cracking occurs due to mechanical fatigue damage.

3. The process zone model semiquantitatively predicts the shape of the  $da/dN$ - $\Delta K$  relationship. For any environment, the FCP law is determined by the  $\Delta K$  dependency and proportion ( $\Theta_i$ ) of each parallel microscopic cracking mode according to:

$$da/dN_{ENV} \propto \Theta_{\{111\}} \Delta K^{2/\beta} + \Theta_{\{100\}} \Delta K^{(2 + 2\phi_{\{100\}})} + \Theta_{SGC} \Delta K^{(2 + 2\phi_{SGC})}$$

and including "plateau" behavior. These exponents are predicted based on the plastic strain range dependencies of  $\Delta a$  and  $\Delta N$  for each damage mechanism. Absolute values of the exponents and the preexponential coefficients are not independently predicted; based on FCP data for alloy 2090:

$$da/dN_{Moist\ Air} = \Theta_{\{111\}}(3 \times 10^{-9}) \Delta K^{4.0} + \Theta_{\{100\}}(1 \times 10^{-8}) \Delta K^{5.1} + \Theta_{SGC}(2 \times 10^{-7}) \Delta K^{2.4}$$

$$da/dN_{Anodic\ NaCl} = \Theta_{\{100\}}(1.7 \times 10^{-7}) \Delta K^{5.1} + \Theta_{SGC}(7 \times 10^{-7}) \Delta K^{2.7}$$

$$da/dN_{Inert} = \Theta_{\{111\}}(3 \times 10^{-9}) \Delta K^{4.0} \quad \text{where } \Theta_{\{111\}} = 1.0$$

$\Theta_i$  values, from fractographic analyses for each cracking mode, are in good agreement with these equations.

4. The process zone model does not quantitatively predict  $da/dN_{ENV}$  values because the local failure criterion for hydrogen cracking is not independently determined, the very near tip

plastic strain distribution is not quantitatively defined, and crack tip dislocation structures are not well characterized. The mechanisms by which hydrogen promotes {100} and intersubgranular cracking are speculative.

5. Crack growth rates increase and the stress intensity required for the microscopic mode transition decreases as the environmentally produced crack surface hydrogen concentration increases. Crack surface films, produced by cathodic polarization in NaCl or O<sub>2</sub> addition to water vapor, reduce hydrogen uptake and da/dN. Bulk hydrogen diffusion in the process zone can augment dislocation transport for slow rate FCP.
6. For 2090 (and other 2000 series alloys) in NaCl, da/dN increases with increased loading frequency because increased crack tip strain rate destabilizes otherwise protective surface films, and enhances hydrogen uptake in the process zone. Fast crack surface chemical reactions, short process zone diffusion distances and rapid dislocation transport of hydrogen preclude rate limited cracking for frequencies less than about 150 Hz.

## VI. ACKNOWLEDGEMENTS

This research was supported by the NASA-Langley Research Center, under Grant NAG-1-745 with D.L. Dicus as program monitor, and by the Virginia CIT Center for Electrochemical Science and Engineering at the University of Virginia. Drs. M.F. Henry, Sang-Shik Kim, J.C. Newman, A.P. Reynolds, E.A. Starke, Jr., G.E. Stoner and J.A. Wert provided important inputs to this work. These contributions are gratefully acknowledged.

## VII. APPENDICES

### A. Determination of the Coefficient $\alpha$ :

The coefficient,  $\alpha$ , is described in Equation 4 and must be determined to calculate the crack advance distance,  $\Delta a$ . It is only possible to estimate  $\Delta\epsilon_{crit}$  and thus  $\alpha$ . Assuming that a critical plastic strain range ( $\Delta\epsilon_p$ ) of between 0.2% and 1% is necessary for significant crack tip plasticity,  $\alpha$  will vary from 0.8 to 0.4 for peak aged alloy 2090 ( $\sigma_{ys} = 500$  MPa and  $E = 81.5$  GPa<sup>(3)</sup>). In principle  $\Delta\epsilon_{crit}$  can be determined from the implication that the threshold  $\Delta K_{th}$  for FCP represents the condition where the peak plastic strain range is just sufficient for damage based on dislocation activity.  $\Delta K_{th}$  may be related to peak  $\Delta\epsilon_p$  through either Equation 3, or based on an extrapolation of SEM measurements of crack tip strains<sup>(8,78)</sup>:

$$\Delta\epsilon_p = K_o (\Delta K - \Delta K_{th}^*)^r \quad (A1)$$

where  $K_o$ ,  $r$  and  $\Delta K_{th}^*$  are curve fit constants for a given alloy and environment. The singularity in strain as  $r$  approaches zero at the crack tip confounds the use of Equation 3; however,  $\Delta\epsilon_{crit}$  equals 0.4% for an assumed threshold of  $3.5 \text{ MPa}\sqrt{\text{m}}$  and an  $r$  of  $2 \mu\text{m}$  ( $\sigma_{ys} = 500$  MPa and  $E = 81.5$  GPa). This  $r$ , the spatial resolution of the SEM method, is selected for comparison with the prediction of Equation A1 and this threshold is a typical value for FCP in 2000 and 7000 alloys in vacuum<sup>(3,5,45)</sup>. For 7075 in vacuum,  $K_o = 1.3 \times 10^{-4}$ ,  $\Delta K_{th}^* = 0$  and  $r = 3.0$  in Equation A1; the corresponding plastic strain range equals 0.6% at a  $\Delta K_{th}$  of  $3.5 \text{ MPa}\sqrt{\text{m}}$ <sup>(8,78)</sup>. From Equation 4,  $\alpha$  equals 0.6 and 0.5, respectively, for these two estimates of the critical plastic strain.

These estimates are not rigorous. The SEM measurements for Equation A1 are variable, do not consider crack closure effects on  $\Delta K$ , are limited to the specimen free surface, must be extrapolated to yield the strain level at threshold, and are likely to depend on the fatigue cracking mode. The use of a vacuum  $\Delta K_{th}$  in Equation 3 is justified only if it corresponds to the threshold dislocation activity for hydrogen accumulation. The use of  $\Delta K_{th}$  for water vapor or chloride bearing environments is unreasonable because bulk hydrogen diffusion may be dominant for low crack growth rates and small process zone sizes typical of near-threshold FCP. This is the reason why  $\Delta K_{th}$  decreases with increasing crack surface hydrogen content, while the dislocation transport concept implies that  $\Delta K_{th}$  and  $\Delta\epsilon_{crit}$  are environment independent.

## B. Analysis of Crack Tip Opening Stress:

Tensile stresses,  $\sigma_N$ , normal to the crack plane and decreasing with increasing distance,  $r$ , from the crack tip may govern interfacial and "cleavage" cracking modes. Continuum analysis shows that  $\sigma_N$  at maximum load is uniformly high (equaling 3 to 4 times  $\sigma_{ys}$ ) over a distance of about  $10 \text{ CTOD}_{\max}^{(40)}$ . Given that:

$$\text{CTOD}_{\max} = \Gamma K_{\max}^2 / \sigma_{ys} E \quad (\text{B1})$$

a yield strain of 0.6% ( $\sigma_{ys}/E$  for 2090) and  $\Gamma$  equalling 0.5<sup>6</sup>, the distance for high  $\sigma_N$  can be restated in terms of  $d_{cz}$ :

$$10 \text{ CTOD}_{\max} = \{1.2/[\alpha(1 - R)^2]\} d_{cz} \quad (\text{B2})$$

When  $\alpha$  equals 0.5,  $\sigma_N$  is high over  $3 d_{cz}$  at a stress ratio of 0.1 and over  $250 d_{cz}$  for  $R$  equaling 0.9. This latter value is typical of the FCP experiments conducted with alloy 2090<sup>(3)</sup>.

## C. Determination of the Relationship Between $\Delta N$ and $\Delta K$ :

In the process zone model, crack advance is presumed to occur over a distance,  $\Delta a$ , when  $\Delta N$  equals the number of load cycles sufficient to achieve the critical trapped hydrogen concentration within the crack tip process zone,  $d_{cz}$ . To determine the  $\Delta K$  dependence of  $\Delta N$ , assume that  $\Delta N$  inversely depends on the total number of mobile dislocations within the embrittlement zone volume,  $N_m$ , raised to some power,  $-\phi$ :

$$\Delta N = \zeta N_m^{-\phi} \quad (\text{C1})$$

where  $\zeta$  is a constant. Since mobile dislocation density ( $\rho$ ) is proportional to plastic strain<sup>(96)</sup>,  $N_m$  equals the product of  $\rho$ ,  $d_{cz}$  and unit process zone thickness. For the more complex case, where  $\Delta \epsilon_p$  depends on distance ahead of the crack tip,  $N_m$  is described by the integral of the plastic strain range distribution from the crack tip to  $d_{cz}$ , per unit process zone thickness. That is:

---

<sup>6</sup>The proportionality constant,  $\Gamma$ , varies between 0.4 (finite element) and 1.0 (Dugdale strip yield) depending on the method of crack tip field analysis<sup>(40)</sup>.

$$N_m = \int_{x^*}^{\alpha d_{cpz}} \Delta \epsilon_p(x) dx \quad (C2)$$

The plastic strain distribution ahead of the crack tip is given in Equation 3.  $x^*$  is a small distance from the crack tip where the continuum analysis predicts a strain singularity, but within which the actual strain is finite and perhaps a constant. Substituting the expression for  $\Delta \epsilon_p(x)$  into Equation C2 and integrating yields:

$$N_m = [\omega \sigma_{ys}/E] \left[ \left\{ \frac{(n+1) \alpha^{n/(n+1)} d_{cpz}/n}{\{(n+1) d_{cpz}^{1/(n+1)} x^{*n/(n+1)}\}/n} \right\} \left\{ 1 - (n \alpha^{1/(n+1)}) / (n+1) \right\} - \right. \\ \left. + x^* \right] \quad (C3)$$

For low work hardening materials such as Al-Li-Cu,  $n$  is on the order of 0.1, for  $\alpha = 0.5$  from Equation 4, and for  $\omega = 1.0$ ; Equation C3 is simplified to:

$$N_m = [\sigma_{ys}/E] [0.8 d_{cpz} - 11.0 x^{*0.09} d_{cpz}^{0.9} + x^*] \quad (C4)$$

Since  $d_{cpz}$  is proportional to  $\Delta K^2$  (Footnote 2), and for small  $x^*$  on the order of 0.05 times  $d_{cpz}$ :

$$N_m = 0.02 \Delta K^2 / \sigma_{ys} E \quad (C5)$$

Combining Equations C5 and C1 yields the  $\Delta K$  dependence of  $\Delta N$  for a low work hardening material ( $n = 0$ ):

$$\Delta N = \zeta' \sigma_{ys}^\phi E^\phi / \Delta K^{2\phi} \quad (C6)$$

## VIII. REFERENCES

1. P.L. Andresen, R.P. Gangloff, L.F. Coffin and F.P. Ford, Fatigue '87, Vol. III-A, R.O. Ritchie and E.A. Starke, Jr., eds., EMAS, West Midlands, UK, pp. 1723-1751 (1987).
2. R.P. Wei and R.P. Gangloff, Fracture Mechanics: Perspectives and Directions, ASTM STP 1020, R.P. Wei and R.P. Gangloff, eds., ASTM, Philadelphia, PA, pp. 233-264 (1989).
3. R.S. Piascik and R.P. Gangloff, Metall. Trans. A, Vol. 22A, pp. 2415-2428 (1990).
4. R.S. Piascik and R.P. Gangloff, "Environmental Fatigue Crack Propagation in Al-Li-Cu Alloy: Part II - Microscopic Hydrogen Cracking Processes", NASA TM-10762 (1992).
5. R.P. Gangloff, Environment Induced Cracking of Metals, R.P. Gangloff and M. Ives, eds., NACE, Houston, TX, pp. 55-109 (1990).
6. N.J.H. Holroyd and D. Hardie, Corrosion Science, Vol. 23, No. 6, pp. 527-546 (1983).
7. K.S. Shin and S.S. Kim, Effects of Hydrogen on Material Behavior, A.W. Thompson and N.R. Moody, eds., TMS, Warrendale, PA, pp. 919-928 (1990).
8. D.L. Davidson and J. Lankford, Fat. Engr. Mat. and Struct., Vol. 6, No. 3, pp. 241-256 (1983).
9. J. Petit and A. Zeghloul, Environmentally Assisted Cracking: Science and Engineering, ASTM-STP 1049, W.B. Lisagor, B.N. Leis and T.W. Crooker, eds., ASTM, Philadelphia, PA, pp. 334-346 (1989).
10. J. Lankford and D.L. Davidson, Acta Metall., Vol. 31, No. 8, pp. 1273-1284 (1983).
11. C.P. Dervenis, E.I. Meletis and R.F. Hochman, Mat. Sci. Engr., Vol. 102, pp. 151-160 (1988).
12. D.J. Duquette, "Mechanisms of Corrosion Fatigue of Aluminum Alloys", AGARD Report No. AGARD-CP-316 (1981).
13. S.W. Ciaraldi, J.L. Nelson, R.A. Yeske and E.N. Pugh, Hydrogen Effects in Metals, I. Bernstein and A.W. Thompson, eds., AIME, Warrendale, PA, pp. 437-447 (1981).
14. W. Gruhl, Z. Metallkde, Vol. 75, pp. 819-926 (1984).
15. A. Niegel, H.-J. Gudladt and V. Gerold, Fatigue '87, R.O. Ritchie and E.A. Starke, Jr., eds., EMAS, West Midlands, UK, pp. 1229-1238 (1987).
16. A. Niegel, H.-J. Gudladt and V. Gerold, J. de Physique, Colloque C5, Vol. 49, pp. 659-663 (1988).
17. Z.-X. Tong, S. Lin and C.-M. Hsiao, Metall. Trans. A, Vol. 20A, pp. 925-933 (1989).
18. G.M. Scamans, Hydrogen Effects in Metals, I.M. Bernstein and A.W. Thompson, eds., TMS-AIME, Warrendale, Pa, pp. 467-475 (1981).
19. C.D.S. Tuck, Hydrogen Effects in Metals, I.M. Bernstein and A.W. Thompson, eds., TMS-AIME, Warrendale, Pa, pp. 503-511 (1981).
20. G. Scamans and C.D.S. Tuck, Environment-Sensitive Fracture of Engineering Materials, Z.A. Foroulis, ed., TMS-AIME, Warrendale, PA, pp. 464-483 (1979).
21. R.E. Ricker and D.J. Duquette, Metall. Trans. A, Vol. 19A, pp. 1775-1783 (1988).

22. S.W. Ciaraldi, J.L. Nelson, R.A. Yeske and E.N. Pugh, Hydrogen Effects in Metals, I.M. Bernstein and A.W. Thompson, eds., AIME, Warrendale, PA, pp. 437-447 (1981).
23. L. Christodoulou and H.M. Flower, Hydrogen Effects in Metals, I.M. Bernstein and A.W. Thompson eds., TMS-AIME, Warrendale, Pa, pp. 493-501 (1981).
24. C.D.S Tuck, Metall. Trans., Vol. 16A, pp. 1503-1514 (1985).
25. L. Christodoulou and H.M Flower, Acta Metall., Vol. 28, pp. 481-487 (1980).
26. J. Albrecht, I.M. Bernstein and A.W. Thompson, Metall. Trans. A, Vol. 23A, pp. 811-820 (1982).
27. D. Nguyen, A.W. Thompson and I.M. Bernstein, Acta Metall., Vol.35, No. 10, pp. 2417-2425 (1987).
28. M. Gao, P.S. Pao and R.P. Wei, Metall. Trans. A, Vol. 19A, pp. 1739-1750 (1988).
29. N.J.H. Holroyd, Environment Induced Cracking of Metals, R.P. Gangloff and M. Ives, eds., NACE, Houston, TX, pp. 311-345 (1990).
30. K.J. Nix and H.M. Flower, Acta Metall., Vol. 23, pp. 841-848 (1975).
31. N. Ohrloff, A. Gysler and G. Luetjering, Journal de Physique, Colloque C3, Suppl. 9, pp. C3-801-807 (1987).
32. E.I. Meletis and W. Huang, Mats. Sci. Engr., Vol. A148, pp. 197-209 (1991).
33. H.K. Birnbaum, Environment Induced Cracking of Metals, R.P. Gangloff and M. Ives, eds., NACE, Houston, TX, pp. 21-29 (1990).
34. G.M. Bond, I.M. Robertson and H.K. Birnbaum, Acta Metall., Vol. 35, pp. 2289-2296 (1987).
35. R.P. Gangloff and D.J. Duquette, Chemistry and Physics of Fracture, R.M. Latanision and R.H. Jones, eds., Martinus Nijhoff Publishers, Dordrecht, Netherlands, pp. 612-645 (1987).
36. N.M. Grinberg, Intl. J. Fatigue, pp. 83-95, April (1982).
37. H.L. Marcus, J.C. Williams and N.E. Paton, Corrosion Fatigue: Chemistry, Mechanics and Microstructure, NACE-I, O. Devereux, A.J. McEvily, and R.W. Staehle, eds., NACE, Houston, TX, pp. 346-358 (1972).
38. F.P. Ford, Corrosion, Vol. 35, pp. 281-287 (1979).
39. F.P. Ford, Environment Induced Cracking of Metals, R.P. Gangloff and M. Ives, eds., NACE, Houston, TX, pp. 139-165 (1990).
40. W.W. Gerberich and S. Chen, Environment Induced Cracking of Metals, R.P. Gangloff and M.B. Ives, eds., NACE, Houston, TX, pp. 167-187 (1990).
41. S.B. Chakraborty, Fat. Engr. Mats. Struct., Vol. 2, pp. 331-344 (1979).
42. D.L. Davidson, Acta Metall., Vol. 32, pp. 707-714 (1984).
43. R.P. Wei, P.S. Pao, R.G. Hart, T.W. Weir and G.W. Simmons, Metall. Trans. A, Vol. 11A, pp. 151-158 (1980).
44. R.P. Wei, "Corrosion Fatigue Crack Growth and Reactions with Bare Steel Surfaces", Corrosion 89, Paper No. 569, NACE, Houston, TX (1989).

45. R.S. Piascik, "Mechanisms of Intrinsic Damage Localization During Corrosion Fatigue: Al-Li-Cu System", PhD Dissertation, University of Virginia, Charlottesville, VA (1990).
46. T.W. Weir, G.W. Simmons, R.G. Hart and R.P. Wei, Scripta Metall., Vol. 14, pp. 357-364 (1980).
47. P.S. Pao, Ming Gao and R.P. Wei, Basic Questions in Fatigue, Vol. II, ASTM STP 924, R.P. Wei and R.P. Gangloff, eds., ASTM, Philadelphia, PA, pp. 182-195 (1988).
48. True-Hwa Shih and R.P. Wei, Engr. Frac. Mech., Vol. 18, pp. 827-837 (1983).
49. R. Nakai, A. Alavi and R.P. Wei, Metall. Trans. A, Vol. 19A, pp. 543-548 (1988).
50. A.M. Green and J.F. Knott, Advances in Fracture Research, Vol. 2, K. Salama, K. Ravi-Chandar, D.M.R. Taplin and P. Rama Rao, eds., Pergamon Press, New York, pp. 1747-1756 (1989).
51. R.J. Gest and A.R. Troiano, Corrosion, Vol. 30, No. 8, pp. 274-279 (1974).
52. K. Papp and E. Kovacs-Csentenji, Scripta Metall., Vol. 15, pp. 161-164 (1981).
53. R.A. Outlaw, D.T. Peterson and F.A. Schmidt, Scripta Metall., Vol. 16, pp. 287-292 (1982).
54. G.M. Scammans and C.D.S. Tuck, Mechanisms of Environment Sensitive Cracking of Materials, P.R. Swann, F.P. Ford, and A.R.C. Westwood, eds., The Metals Soc., London, pp. 482-91 (1977).
55. P.N. Anyalebechi, Metall. Trans. B, Vol. 21B, pp. 649-655 (1990).
56. A.W. Thompson and I.M. Bernstein, Advances in Corrosion Science and Technology, Vol. 2, M.G. Fontana and R.W. Staehle, eds., Plenum Press, New York, NY, pp. 153-175 (1980).
57. G.S. Chen and D.J. Duquette, "The Effect of Ageing on the Hydrogen-Assisted Fatigue Cracking of a Precipitation Hardened Al-Li-Zr Alloy", PhD Dissertation, Rensselaer Polytechnic Institute, Troy, NY (1991).
58. J.P. Hirth, Metall. Trans. A, Vol. 11A, pp. 861-890 (1980).
59. J.K. Tien, A.W. Thompson, I.M. Bernstein and R.J. Richards, Metall. Trans. A, Vol. 7A, pp. 821-829 (1976).
60. E.A. Starke, Jr., and G. Lutering, Fatigue and Microstructure, ASM, Metals Park, OH, pp. 205-243 (1979).
61. R.J.H. Wanhill and L. Schra, "Corrosion Fatigue Crack Arrest in Aluminum Alloys", NLR Report NLR TR 87128 U, National Aerospace Laboratory, Amsterdam, Netherlands (1987).
62. G.R. Yoder, L.A. Cooley and T.W. Crooker, Fracture Mechanics: Fourteenth Symposium ASTM STP 791, J.C. Lewis and G. Sines, eds., Vol. 1, ASTM, Philadelphia, PA, pp. 313-349 (1983).
63. G.R. Yoder, L.A. Cooley and T.W. Crooker, Scripta Metall., Vol. 16, pp. 1021-1025 (1982).
64. B.R. Kirby and C.J. Beevers, Fat. Engr. Matls. Struct., Vol. 1, pp. 203-215 (1979).
65. H.-J. Gudladt, A. Niegel and P. Liang, Proc. Matls. Res. Soc., Vol. 122, MRS, Boston, MA, pp. 405-409 (1988).
66. C.D.S. Tuck, Hydrogen Effects in Metals, I.M. Bernstein and A.W. Thompson, eds., TMS-AIME, Warrendale, Pa, pp. 503-511 (1981).

67. Fu-Shiong Lin and E.A. Starke, Jr., Matls. Sci. and Engr., Vol. 43, pp. 65-76 (1980).
68. D.L. Davidson and J. Lankford, "Fatigue Crack Growth in Metals and Alloys", Intl. Matls. Rev., to be published (1992).
69. W.W. Gerberich, D.L. Davidson, X.F. Chen and C.S. Lee, Engr. Fract. Mech., Vol. 28, pp. 505-518 (1987).
70. C. Laird, Fatigue Crack Propagation, ASTM STP 415, ASTM, Philadelphia, PA, pp. 131-168 (1967).
71. R.M. Pelloux, Trans. ASM, Vol. 62, pp. 281-284 (1969).
72. P.J.E. Forsyth and D.A. Ryder, Metallurgia, Vol. 63, pp. 117-124 (1961).
73. J.A. Feeney, J.C. McMillan and R.P. Wei, Met. Trans., Vol. 1, pp. 1741-1757 (1970).
74. D.A. Meyn, Met. Trans., Vol. 2, pp. 853-865 (1971).
75. P.J.E. Forsyth, Acta Metall., Vol. 11, pp. 703-716 (1963).
76. C.A. Stubbington, Metallurgia, Vol. 65, pp. 109-121 (1963).
77. R.E. Stoltz and R.M. Pelloux, Met. Trans., Vol. 3, pp. 2433-2441 (1972).
78. D.L. Davidson and J. Lankford, High Strength Powder Metallurgy Aluminum Alloys II, G.J. Hildeman and M.J. Koczak, eds., TMS-AIME, Warrendale, PA, pp. 47-59 (1986).
79. E.A. Starke, Jr., F.S. Lin, R.T. Chen and H.C. Heikkinen, Fatigue Crack Growth Threshold Concepts, D. Davidson and S. Suresh, eds., TMS-AIME, Warrendale, PA, pp. 43-61 (1984).
80. J.M. Duva, M.A. Daeubler, E.A. Starke, Jr. and G. Luetjering, Acta Metall., Vol. 36, pp. 585-589 (1987).
81. Ravi Krishnamurthy, "Microstructure and Yield Strength Effects on Hydrogen Environment Enhanced Fatigue of Steels", PhD Dissertation, University of Virginia, Charlottesville, VA (1991).
82. W.W. Gerberich, D.L. Davidson and M. Kaczorowski, J. Mech. Phys. Solids, Vol. 38, pp. 87-113 (1990).
83. H.J. Roven, "Cyclic Deformation and Fatigue Crack Propagation in a Low Alloyed Steel", PhD Dissertation, Norwegian Institute of Technology, Trondheim, Norway (1988).
84. H.J. Roven and E. Nes: Acta Metall. Mater., Vol. 39, pp. 1735-1754 (1991).
85. J. Petit, Fatigue Crack Growth Threshold Concepts, D. Davidson and S. Suresh, eds., AIME, Warrendale, PA, pp. 3-24 (1984).
86. G.M. Pressouyre, Acta Metall., Vol. 28, pp. 895-911 (1980).
87. J.R. Scully, J.A. Van Den Avyle, M.J. Cieslak, A.D. Romig, Jr. and C.R. Hills, Metall. Trans. A, Vol. 22A, pp. 2429-2444 (1991).
88. Seong-Min Lee and Su-II Pyun, Scripta Metall., Vol. 24, pp. 1629-1634 (1990).
89. R.G. Buchheit, Jr., J.P. Moran and G.E. Stoner, Corrosion, Vol. 46, pp. 610-617 (1990).
90. A.P. Reynolds and G.E. Stoner, Metall. Trans. A, Vol. 22A, pp. 1849-1855 (1991).

91. G.G. Garrett and J.F. Knott, Acta Metall., Vol. 23, pp. 841-848 (1975).
92. S.P. Lynch, Scripta Metall., Vol. 20, pp. 1067-1072 (1986).
93. P. Neumann, Acta Metall., Vol. 22, pp. 1155-1178 (1974).
94. R. Balasubramaniam, D.J. Duquette, and K. Rajan, Acta Metall. Mater., Vol. 39 No. 11, pp. 2607-2613 (1991).
95. R. Balasubramaniam, D.J. Duquette, and K. Rajan, Acta Metall. Mater., Vol. 39 No. 11, pp. 2597-2605 (1991).
96. T.H. Courtney, Mechanical Behavior of Materials, McGraw-Hill Publishing Co., New York, pp. 128-131 (1990).
97. P.S. Pao, Ming Gao and R.P. Wei, Scripta Metall., Vol. 43, No. 4, pp. 204-207 (1987).
98. B.R.W. Hinton and R.P.M. Procter, Metals Forum, Vol. 5, pp. 80-91 (1982).
99. K.T. Venkateswara Rao and R.O. Ritchie, "Fatigue of Aluminum-Lithium Alloys", University of California, Report No. LBL-30176, Berkeley, CA (1991).
100. R.G. Buchheit, Jr., J.P. Moran and G.E. Stoner, "The Role of Hydrolysis in the Crevice Corrosion of Al-Li-Cu Alloys" Corrosion 90, Paper No. 90093, NACE, Houston, TX (1990).
101. K. Sotoudeh, T.H. Nguyen, R.T. Foley and B.F. Brown, Corrosion, Vol. 72, pp. 301-304 (1981).
102. D.W. Sitari and R.C. Alkire, J. Electrochem. Soc., Vol. 129, pp. 488-496 (1982).
103. S.E. Stanzl, H.R. Mayer and E.K. Tschegg, Matls. Sci. and Engr., Vol. 80, to be published (1992).
104. D.L. Davidson and J. Lankford, Matls. Sci. and Engr., Vol. 74, pp. 189-199 (1985).

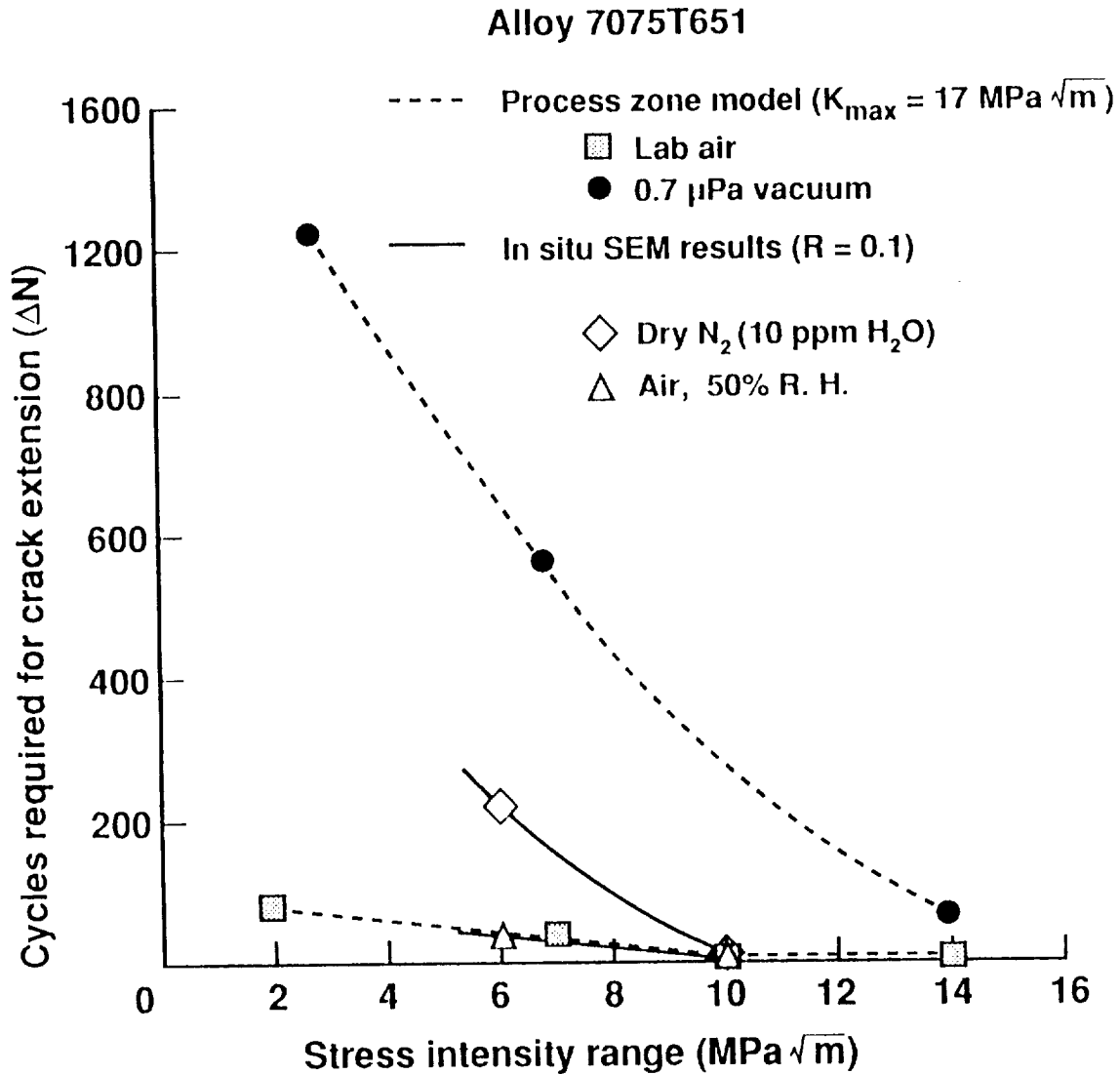


*Figure 1* A comparison of calculated load cycles for discontinuous crack growth in alloy 7075 exposed to either moist air or inert environments.  $\Delta N$  values are based on either the process zone model with measured  $da/dN$ , or SEM measurements of crack tip strain range with a Coffin-Manson failure criterion<sup>(8)</sup>.

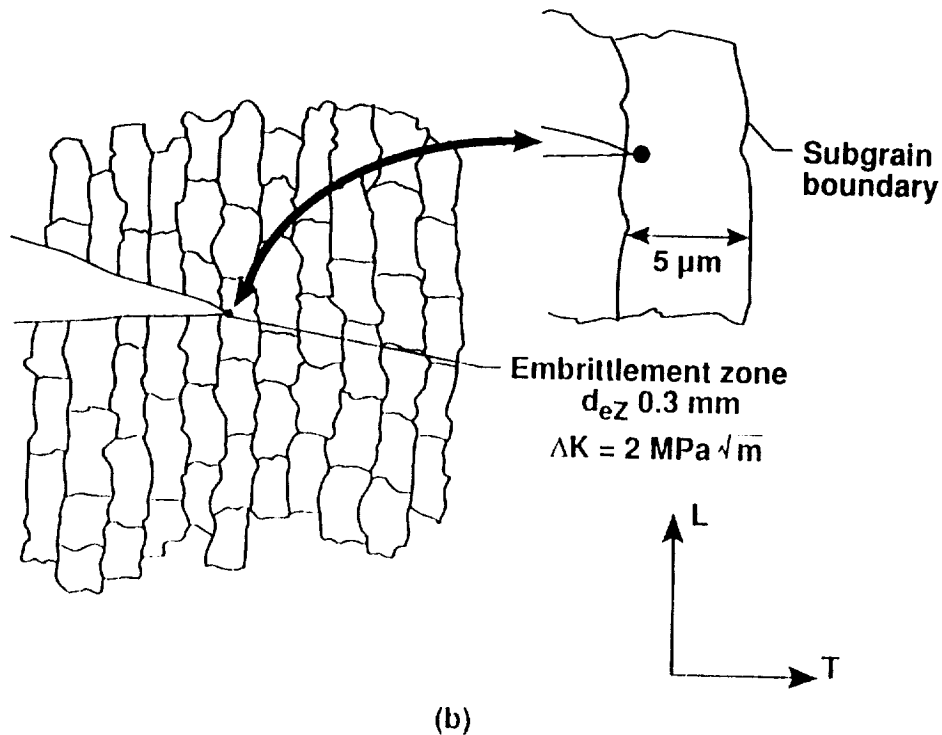
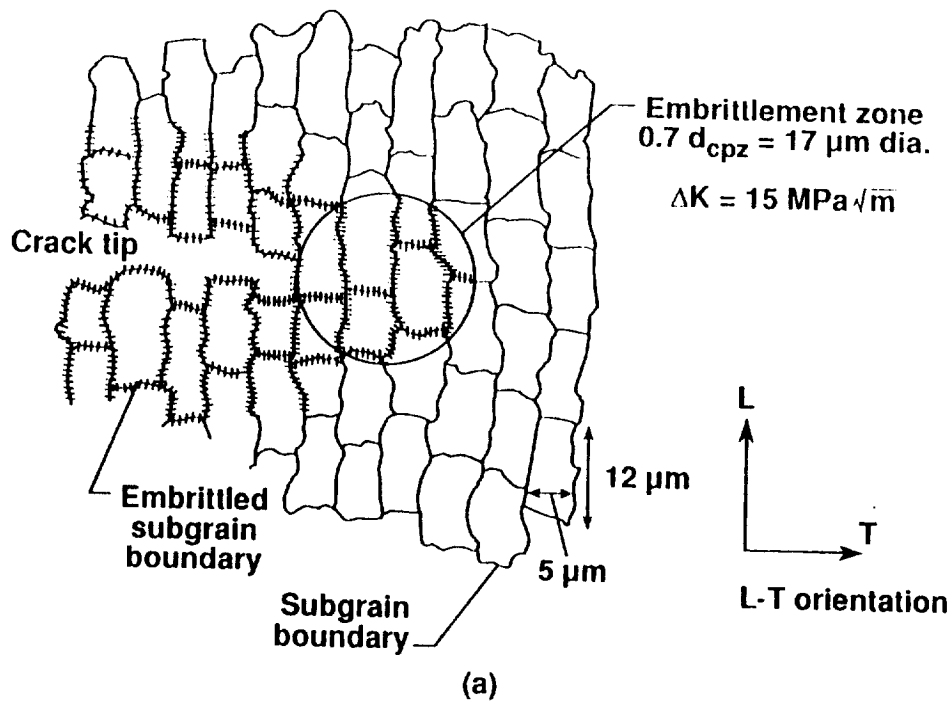


Figure 2

A schematic drawn to scale showing the crack tip process zone at constant  $\Delta K$  for hydrogenous environments; (a) Regions B and C SGC where the embrittlement process zone is larger than subgrain size, and (b) low  $\Delta K$  {100} FCP, Region A in Table I, where the process zone is smaller than the subgrain size.

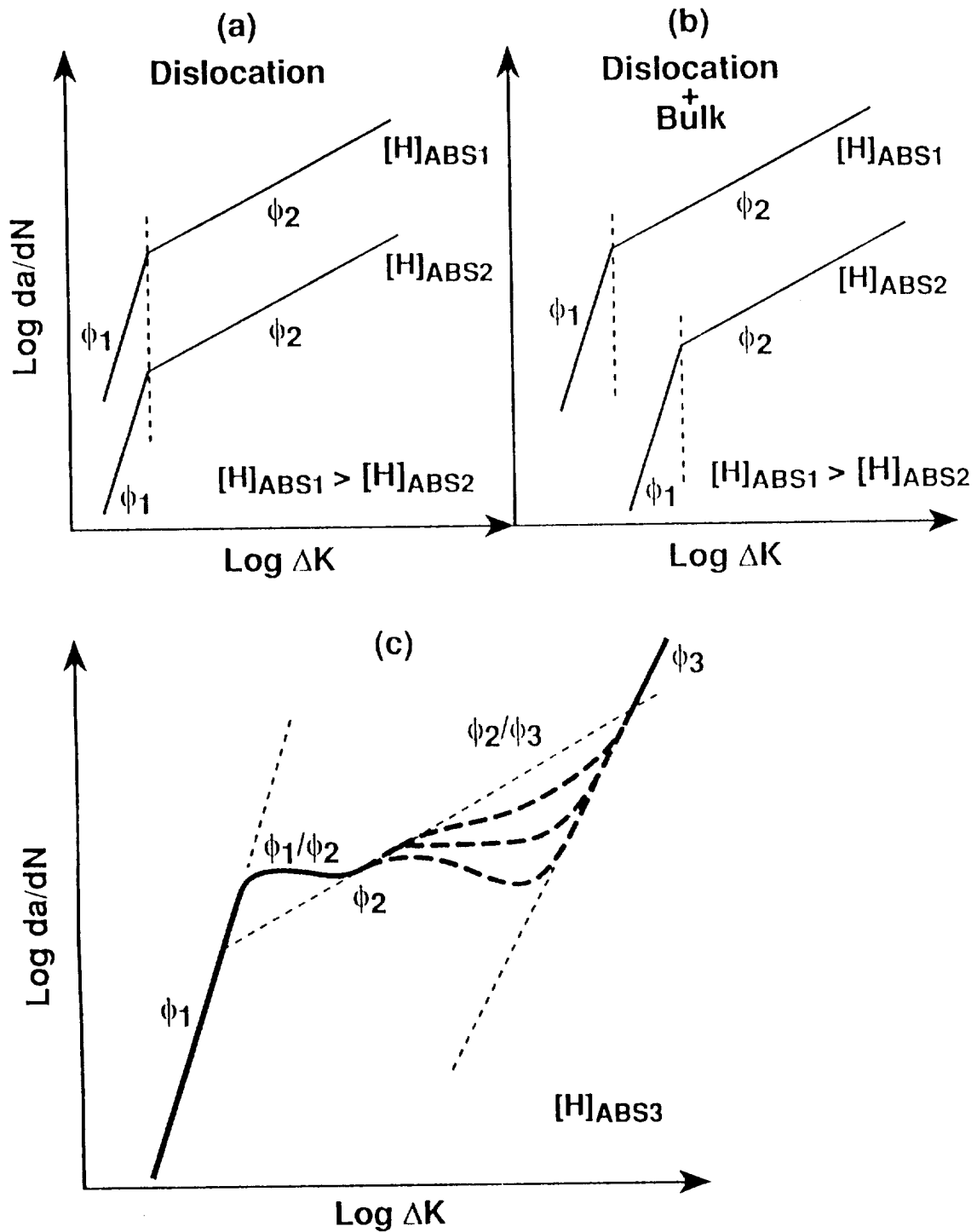


Figure 3

Da/dN versus  $\Delta K$  relationships based on the process zone model for hydrogen enhanced FCP in Al-Li-Cu alloys. (a) and (b) For a transition between single modes of cracking,  $[H]_{\text{ABS}}$  affects FCP for dislocation transport of hydrogen within  $d_{\text{cz}}$  and for dislocation transport augmented by bulk hydrogen diffusion. (c) Complex da/dN- $\Delta K$  relationships result when multiple FCP modes operate in parallel at fixed  $[H]_{\text{ABS}}$ .

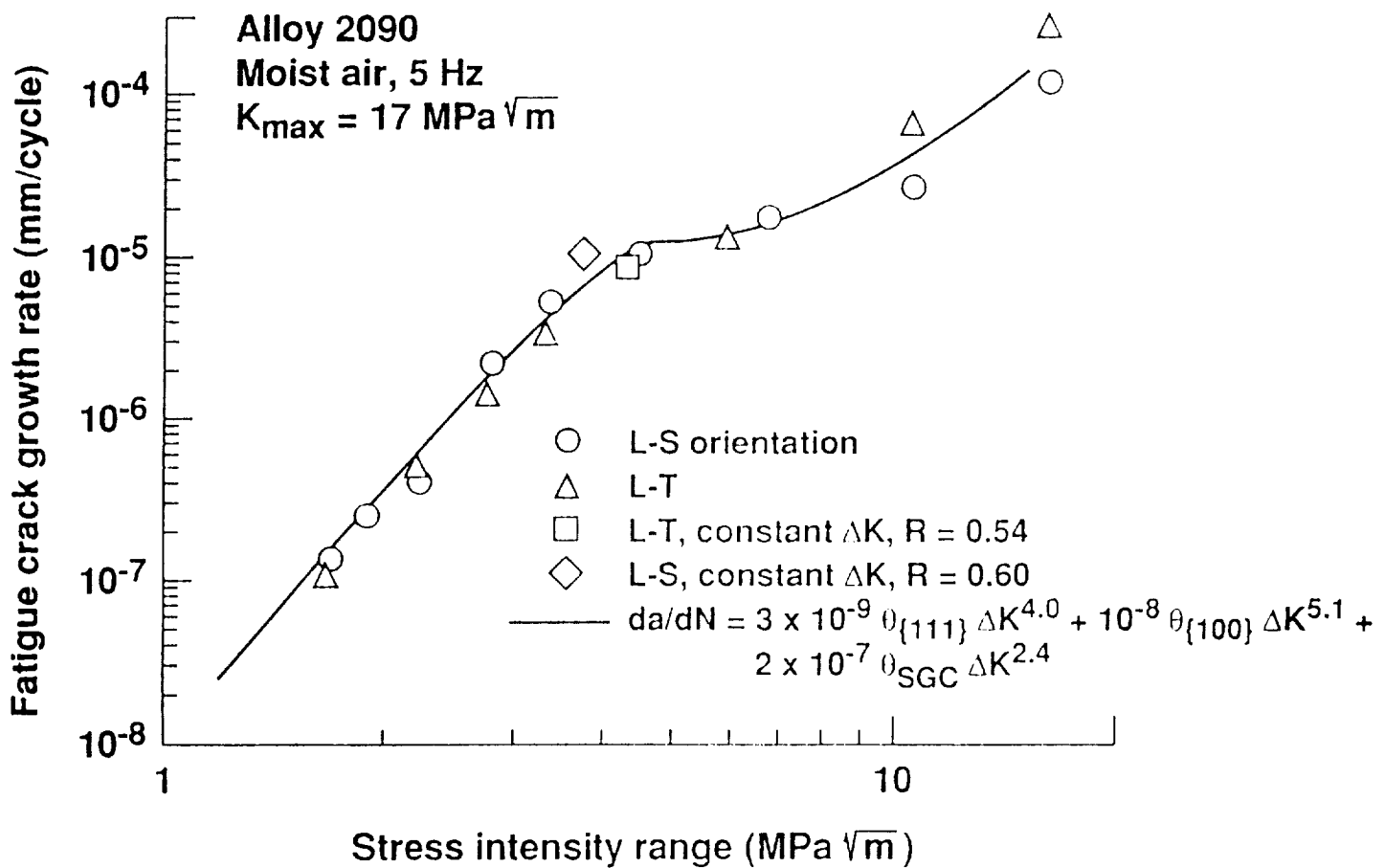


Figure 4 A comparison of measured and predicted  $da/dN$ - $\Delta K$  "plateau" behavior for alloy 2090 in moist air.

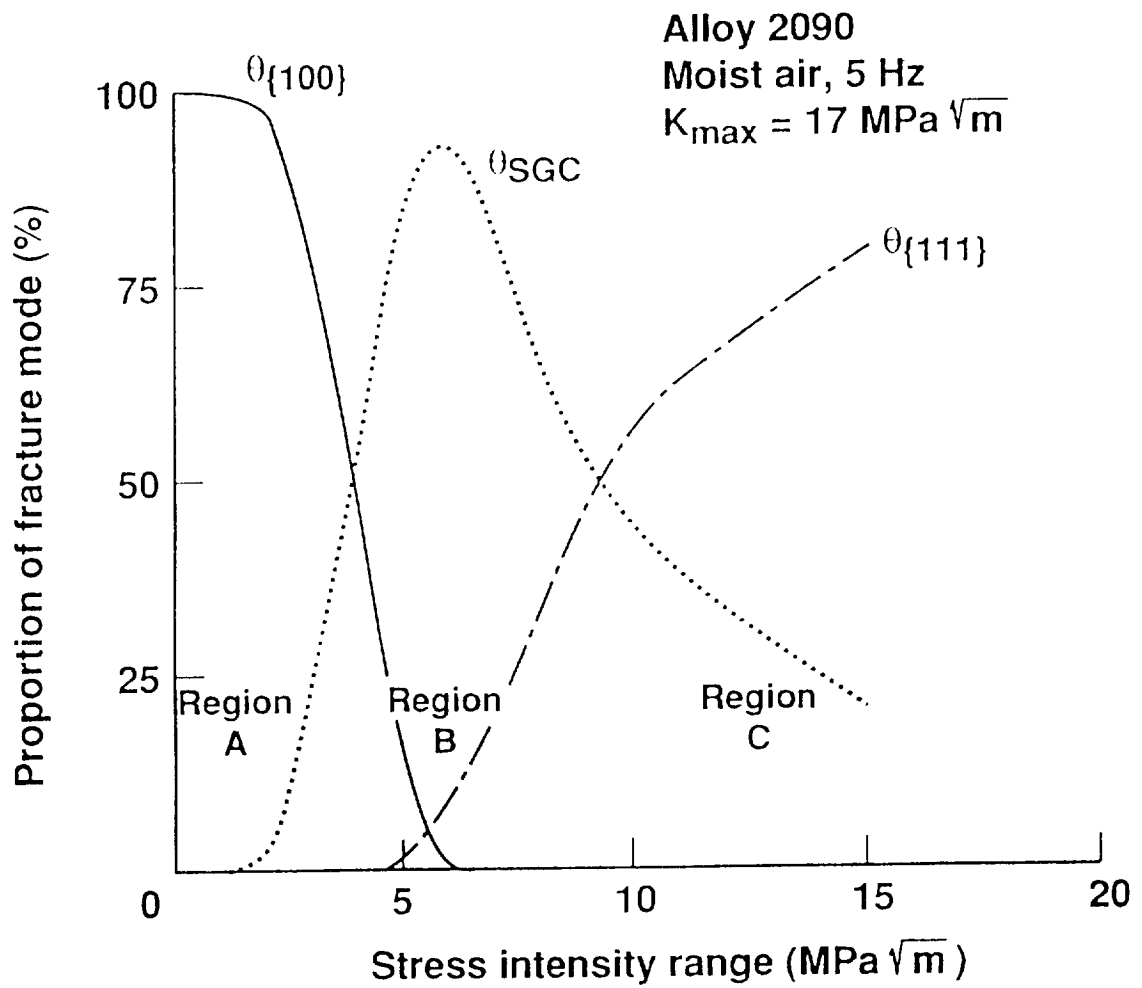
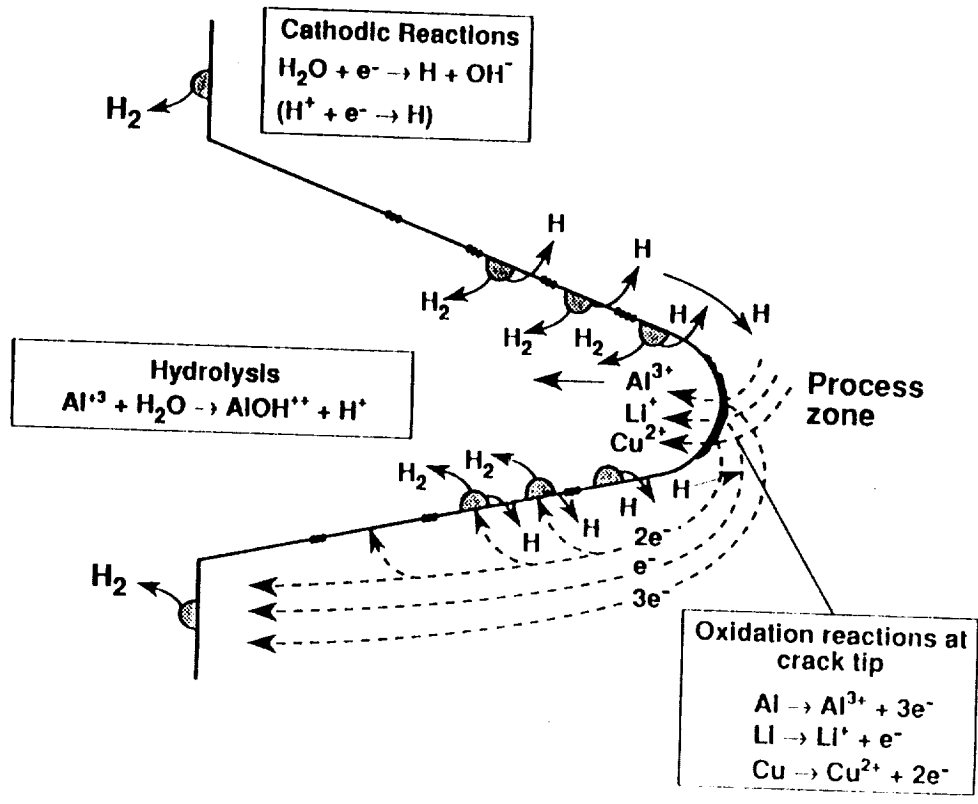
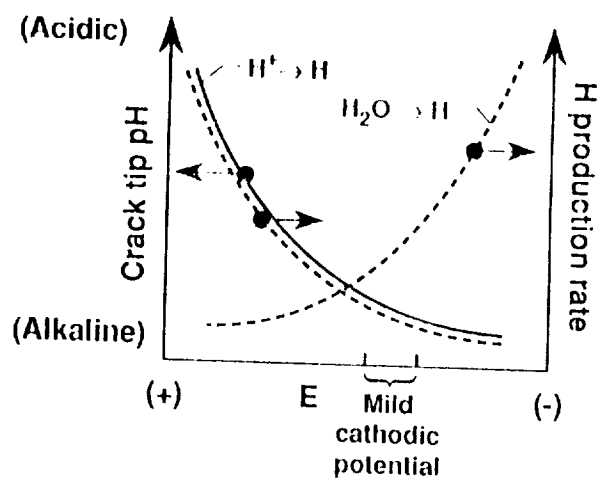


Figure 5 The estimated distributions of  $\Theta_{\{111\}}$ ,  $\Theta_{\{100\}}$  and  $\Theta_{\text{SGC}}$  for alloy 2090 in moist air.



(a)



(b)

Figure 6 A schematic depicting: (a) occluded cell electrochemical reactions in Al-Li-Cu leading to crack surface hydrogen production,  $[H]_{ABS}$ , and (b) crack tip pH and atomic hydrogen production rate as a function of electrode potential.



# REPORT DOCUMENTATION PAGE

Form Approved  
OMB No. 0704-0188

Public reporting burden for this collection of information is estimated to average 1 hour per response, including the time for reviewing instructions, searching existing data sources, gathering and maintaining the data needed, and completing and reviewing the collection of information. Send comments regarding this burden estimate or any other aspect of this collection of information, including suggestions for reducing this burden, to Washington Headquarters Services, Directorate for Information Operations and Reports, 1215 Jefferson Davis Highway, Suite 1204, Arlington, VA 22202-4302, and to the Office of Management and Budget, Paperwork Reduction Project (0704-0188), Washington, DC 20503.

<b>1. AGENCY USE ONLY (Leave blank)</b>	<b>2. REPORT DATE</b> May 1992	<b>3. REPORT TYPE AND DATES COVERED</b> Technical Memorandum	
<b>4. TITLE AND SUBTITLE</b> Environmental Fatigue of an Al-Li-Cu Alloy: Part III - Modeling of Crack Tip Hydrogen Damage		<b>5. FUNDING NUMBERS</b>  505-63-50-04	
<b>6. AUTHOR(S)</b> Robert S. Piascik and Richard P. Gangloff			
<b>7. PERFORMING ORGANIZATION NAME(S) AND ADDRESS(ES)</b> NASA Langley Research Center Hampton, VA 23665-5225		<b>8. PERFORMING ORGANIZATION REPORT NUMBER</b>	
<b>9. SPONSORING / MONITORING AGENCY NAME(S) AND ADDRESS(ES)</b> National Aeronautics and Space Administration Washington, DC 20546		<b>10. SPONSORING / MONITORING AGENCY REPORT NUMBER</b>  NASA TM-107619	
<b>11. SUPPLEMENTARY NOTES</b> Piascik: NASA Langley Research Center, Hampton, VA 23665-5225; Gangloff: University of Virginia, Materials Science and Engineering Department, Charlottesville, VA 22903			
<b>12a. DISTRIBUTION / AVAILABILITY STATEMENT</b>  Unclassified - Unlimited  Subject Category - 39		<b>12b. DISTRIBUTION CODE</b>	
<b>13. ABSTRACT (Maximum 200 words)</b> Environmental fatigue crack propagation rates and microscopic damage modes in Al-Li-Cu alloy 2090 (Parts I and II) are described by a crack tip process zone model based on hydrogen embrittlement. $da/dN_{ENV}$ equates to discontinuous crack advance over a distance, $\Delta a$ , determined by dislocation transport of dissolved hydrogen at plastic strains above a critical value; and to the number of load cycles, $\Delta N$ , required to hydrogenate process zone trap sites that fracture according to a local hydrogen concentration-tensile stress criterion. Transgranular {100} cracking occurs for process zones smaller than the subgrain size, and due to lattice decohesion or hydride formation. Inter-subgranular cracking dominates when the process zone encompasses one or more subgrains so that dislocation transport provides hydrogen to strong boundary trapping sites. Multi-sloped $\log da/dN - \log \Delta K$ behavior is produced by process zone plastic strain-hydrogen-microstructure interactions, and is determined by the $\Delta K$ dependent rates and proportions of each parallel cracking mode ( $\theta_i$ ) according to: $da/dN_{ENV} \propto \theta_{\{111\}} \Delta K^{2.1\beta} + \theta_{\{100\}} \Delta K^{(2 + 2\phi - \{100\})} + \theta_{SGC} \Delta K^{(2 + 2\phi - SGC)}$ Absolute values of the exponents and the preexponential coefficients are not predictable; however, fractographic measurements of $\theta_i$ coupled with fatigue crack propagation data for alloy 2090 established that the process zone model correctly describes fatigue crack propagation kinetics. For example: $da/dN_{Moist Air} = \theta_{\{111\}} (3 \times 10^{-9}) \Delta K^{4.0} + \theta_{\{100\}} (1 \times 10^{-8}) \Delta K^{5.1} + \theta_{SGC} (2 \times 10^{-7}) \Delta K^{2.4}$ where each $\theta$ is known as a function of $\Delta K$ . Crack surface films hinder hydrogen uptake to reduce $da/dN$ and alter the proportions of each fatigue crack propagation mode.			
<b>14. SUBJECT TERMS</b> Environmental fatigue; Corrosion fatigue; Aluminum-Lithium; Hydrogen embrittlement; Crack tip modeling		<b>15. NUMBER OF PAGES</b> 41	
		<b>16. PRICE CODE</b> A03	
<b>17. SECURITY CLASSIFICATION OF REPORT</b> Unclassified	<b>18. SECURITY CLASSIFICATION OF THIS PAGE</b> Unclassified	<b>19. SECURITY CLASSIFICATION OF ABSTRACT</b>	<b>20. LIMITATION OF ABSTRACT</b>



